INFORMATION TO USERS

This manuscript has been reproduced from the microfilm master. UMI films the text directly from the original or copy submitted. Thus, some thesis and dissertation copies are in typewriter face, while others may be from any type of computer printer.

The quality of this reproduction is dependent upon the quality of the copy submitted. Broken or indistinct print, colored or poor quality illustrations and photographs, print bleedthrough, substandard margins, and improper alignment can adversely affect reproduction.

In the unlikely event that the author did not send UMI a complete manuscript and there are missing pages, these will be noted. Also, if unauthorized copyright material had to be removed, a note will indicate the deletion.

Oversize materials (e.g., maps, drawings, charts) are reproduced by sectioning the original, beginning at the upper left-hand corner and continuing from left to right in equal sections with small overlaps. Each original is also photographed in one exposure and is included in reduced form at the back of the book.

Photographs included in the original manuscript have been reproduced xerographically in this copy. Higher quality 6" x 9" black and white photographic prints are available for any photographs or illustrations appearing in this copy for an additional charge. Contact UMI directly to order.

UMI

A Bell & Howell Information Company
300 North Zeeb Road, Ann Arbor MI 48106-1346 USA
313/761-4700 800/521-0600

A TESTBED FOR INVESTIGATING THE EFFECT OF ELECTRODE STRUCTURE ON THE PERFORMANCE OF A SOLID OXIDE ELECTROLYSIS SYSTEM

by
Stephen Brod

A Thesis Submitted to the Faculty of the

DEPARTMENT OF AEROSPACE AND MECHANICAL ENGINEERING

In Partial Fulfillment of the Requirements
For the Degree of

MASTER OF SCIENCE
WITH A MAJOR IN AEROSPACE ENGINEERING

In the Graduate College

THE UNIVERSITY OF ARIZONA

1995

STATEMENT BY AUTHOR

This thesis has been submitted in partial fulfillment of requirements for an advanced degree at The University of Arizona and is deposited in the University Library to be made available to borrowers under rules of the Library.

Brief quotations from this thesis are allowable without special permission, provided that accurate acknowledgment of source is made. Requests for permission for extended quotation from or reproduction of this manuscript in whole or in part may be granted by the copyright holder.

SIGNED: Stephen Broad

APPROVAL BY THESIS DIRECTOR

This thesis has been approved on the date shown below:

R. N. Kumar

Dr. Kumar Ramohalli
Professor of Aerospace Engineering

30th Nov. '95

Date

Acknowledgments

Without the following people, this thesis could not have been completed. Thank you.

Dr. Kumar Ramohalli, who provided all those things an advisor is supposed to provide.

Dr. Steve Crow, for support and assistance, and believing I know what I am doing.

Drs. Murray Hirschbein, Gordon Johnston, and Robert Hayduk for support through the UA/ NASA USERC as part of grant NAGW 1332.

Milton Schick, without whom the pieces would not have been put together.

Josie Tanner, who helped keep me sane, and made sure paperwork didn't get in the way.

Chuck Manning and James Lamb, of JPL's Microdevices Lab, for there assistance.

Sarah Dahl, of U of A's Microelectronics Lab, for getting me out of a jam.

Jeannie, Steve, Scott, Jenny, Jen, Leslie, and a few other people, who prevented nervous breakdowns, and were a constant reminder that this stuff is fun. Really it is.

To my parents,

who taught me to reach for the stars,

never realizing that I would take them literally;

to Anne,

whose star will never be forgotton;

and to Alice,

who brought the heavens down to Earth.

TABLE OF CONTENTS

LIST OF ILLUSTRATIONS

LIST OF TABLES

ABSTRACT

In-Situ Resource Utilization (ISRU) can reduce the mass launched to low Earth orbit for a Mars Sample Return Mission by as much as 75%. Solid Oxide Electrolysis is a candidate technology for producing oxygen out of carbon dioxide. A testbed was developed to test the effect of electrode structure on electrode performance. The testbed used all metal interconnects. Electrodes of 0.5 microns (applied by evaporative deposition) and 10-12 microns thick (applied by airbrushing) were produced. The disks were tested in argon, oxygen, and carbon dioxide. The thin electrode showed deterioration in both short term and long term tests. The thick electrode showed no deterioration even over a 120 hour test. Oxygen was produced from carbon dioxide for extended durations. The experiments show the thicker electrode is needed for an oxygen production system. The electrode/electrolyte disks withstood normal handling without damage.

INTRODUCTION

The first people to realize that the planets were other worlds like Earth, were the followers of Pythagoras, in the 6th century BC.[1] Of course, they had made a lucky guess, and were ignored or derided by everyone else. It was not until Galileo obtained a telescope that anyone could tell for certain the planets were worlds, or more accurately, Earth was a planet.

The moon was an obvious exception. A glance told anyone the moon had features. It might glow, but the moon was a world. The first person who is known to have written about a voyage to the moon was Lucian. In the 2nd century, his True History told of an accidental trip to the moon (Talk about a wrong turn!).[1] After his second book, the subject does not appear again until the 1630's, when there was a sudden explosion of books on the subject, including works of fiction by Kepler and Bishop Godwin, and a nonfiction book by Bishop Wilkins, which is the first mention of lunar colonies.[1] One other notable book was Cyrano de Bergerac's Voyages to the Moon and Sun, which contains the first suggestion of using rockets to reach the moon.[1] All these writers assumed if the Moon was a world, and if the planets were worlds, then they must be like Earth, with air and food, and water. All of them assumed travelers to the planets would be able to survive off what they found there.

Today, we know that is not the case. Except for our own planet, every world we know about is hostile. Half the planets in the solar system don't have a surface for anyone to visit. They consist of hydrogen, helium and varying amounts of methane. Pluto, while it does have a surface, also has an atmosphere that is frozen half the time.[2] The moons of the gas giants are more promising.

Water ice is present on many of them, but few have much of an atmosphere. Triton's atmosphere has a density of 1/70,000 of Earth's. Titan does have a nitrogen based atmosphere, but instead of oxygen, it has methane and argon. While it is possible for organic compounds to exist there, the average temperature of -179 °C makes it impossible for them to develop any complexity.[2]

It might be expected the inner terrestrial planets would offer more hope, but unfortunately, they don't. Mercury has an atmosphere 1 trillionth the density of Earth's, and a temperature ranging from 467 °C to -183 °C. Venus is known as Earth's twin, and it's atmospheric density is 95 times Earth's. It also has an average temperature of 482 °C and sulfuric acid clouds moving at 360 kph.[2]

The best hope for humans finding a place to survive is Mars. The temperature can reach as high as -14 °C in the summer, but sinks to -120 °C in the winter. Unfortunately, the atmosphere is only 1 percent as thick as Earth's, and Mars is prone to large dust forms with hurricane speed winds. In addition, what atmosphere there is consists of 95% CO_2, with Nitrogen and Argon making up the balance.[2] Mars may be the nicest spot in the solar system off Earth, but it leaves a lot to be desired as a vacation destination. It is clear whatever humans need to survive must be brought with them. The solar system offers no free lunches (literally), or gas stations.

As we learned more about the solar system, space mission planners needed to supply everything the mission would need, including fuel for the return trip, and food and air for manned missions. As the space pioneers realized this requirement they were not happy. Rockets are expensive, and big rockets are very expensive. Every pound that has to be lifted requires about nine pounds of

fuel. The fuel adds up very quickly. As Hermann Oberth put it, "I was not pleased at all with the enormous fuel consumption."[1] Complex missions require so much material to be launched from Earth that no one can hope to afford the cost. If mankind is to explore the solar system, an alternative is needed.

An answer does exist, and it is not new. We might not be able to breathe and eat what is out there, but maybe we can convert extraterrestrial materials into something we can breathe, and maybe we can grow food in the soil we find. We certainly can make rocket propellants. Goddard himself was the first to suggest mining oxygen and hydrogen from moon rocks.[1] While it turns out hydrogen may not be available in usable quantities, there is enough oxygen in lunar rocks to make any mission planner happy. If recent indications from the Clementine mission turn out to be true, and there is water on the moon, then we would have a large supply of both oxygen and hydrogen within easy reach. Arthur C. Clarke once wrote, "The Moon's surface is already 95% of the way to Mars and Venus. If rocket propellants can be manufactured there - and this could be done simply by electrolyzing lunar water - it could be the key to the Solar System." [1]

Unfortunately, until recently, the idea of using extraterrestrial resources (known as In-Situ Resource Utilization, or ISRU) was not accepted by mission planners. It was not even seriously studied until Ash, Dowler, and Varsi studied the concept in their 1978 paper, "Feasibility of Rocket Propellant Production on Mars." [3] In this paper they suggested using propellants produced on Mars would enable sample return missions to be launched on a direct trajectory back to Earth, eliminating the need for a long distance automated rendezvous and docking maneuver in Martian orbit.[3,4] In addition, later work found ISRU

technologies would make it possible to launch a sample return mission in a single shuttle launch.[5] More recent estimates show such a mission could be launched using an expendable rocket. Richter, et al, showed a 2 to 1 mass advantage for ISRU missions is a conservative figure.[5]

Figure 1 shows the results of a 1992 study by Kaloupis, Nolan, and Cutler. They examined the required mass of a Mars sample return vehicle for H_2/O_2, CH_4/O_2, and CO/O_2 propellant combinations. The first two propellant choices require hydrogen to be carried from Earth. Only the final case uses propellants completely produced on Mars for the home trip. The chart shows the CO/O_2 combination gives a 4 to 1 mass advantage over a conventional H_2/O_2 mission using only propellants launched from Earth.[6] Additional studies have also shown ISRU technologies can drastically reduce the weight of sample return missions.[4,7]

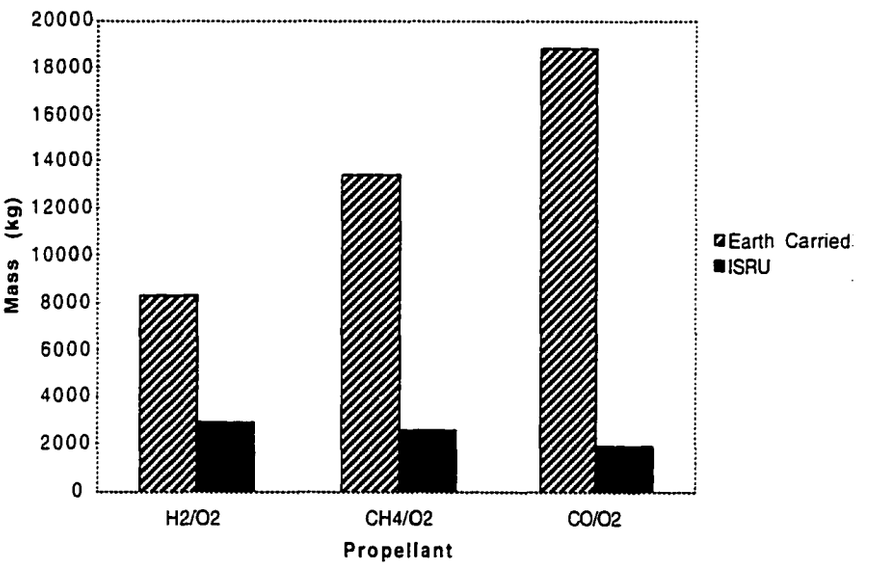

Figure 1. Mass Benefit of ISRU Technologies.

In 1986, the National Commission on Space report considered ISRU to be an important aspect of future space exploration plans.[8]

Most of the studies on ISRU have limited themselves to a Mars sample return mission. These missions were chosen for several reasons. The first is ISRU can only benefit a mission where something is returning to Earth. Obviously, it makes no sense to produce propellant on a planet if you are not going anywhere. Unmanned missions were selected to show the technology could have important benefits on a near-term mission, and to show the technology works, before having people depending on it for survival.

Mars turns out to be an ideal place for ISRU to be implemented. As Ash, et. al., pointed out, Mars is the only place we can use the atmosphere instead of rock to produce propellants, and it is the only place where we know the composition of the feedstock well enough to design systems. Table 1 gives the composition of the Martian atmosphere. We are not required to search for suitable

Table 1. Martian Atmosphere

Gas	%
CO_2	95.3
N_2	2.75
Ar	1.6
O_2	0.13
CO	0.07

from Reference 9

resources since the atmosphere extends more or less uniformly over the entire planet.[9] In addition, the low temperature increases refrigerator efficiency for liquefaction.[3]

The leading technology for producing oxygen from the carbon dioxide in the Martian Atmosphere is Solid Oxide Electrolysis (SOE). Nernst developed the science behind the technology, using zirconia's oxygen ion conducting properties to power a small lamp in 1899.[10] Since that time, it has been found many ceramic oxides selectively conduct oxygen ions at high temperatures. Research into solid oxide fuel cells has been conducted since the 1930's.[10] The electrolysis process reverses the fuel cell, using electrical power to drive chemical reactions. Figure 2 shows a schematic of an electrolysis cell. Carbon dioxide is fed into the apparatus, which operates at a high temperature, usually between

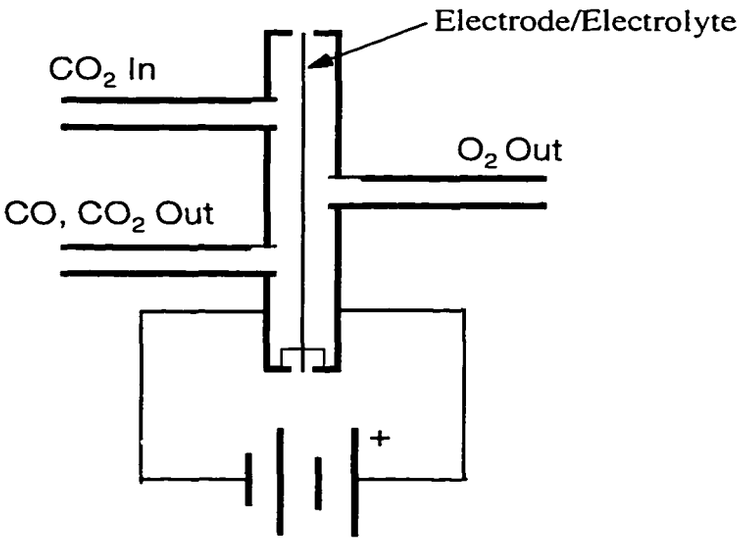

Figure 2. Schematic Diagram of Solid Oxide Electrolysis Cell

900 and 1000 °C. The carbon dioxide interacts with a platinum electrode, and disassociates into carbon monoxide and an oxygen ion. The ion then is attracted to an oxygen vacancy on the electrolyte surface (in our case, yittria stabilized zirconia) and begins its journey through the electrolyte. When it reaches the other side, it gives up an electron, finds another ion that has done the same, and forms an oxygen molecule. The primary products from the system are oxygen on one side of the cell, and a carbon monoxide, carbon dioxide mixture on the other side. The carbon dioxide can be selectively adsorbed from the mixture after leaving the cell, resulting in a pure CO feed that can be used as fuel. The details of the processes involved are described in the next chapter.

It is interesting to note, however, if hydrogen is introduced to the input stream, this process can be adapted to produce methane.[11] Unfortunately, unless water is found on Mars, it will be necessary to carry the hydrogen from Earth. While hydrogen is a very light substance, the equipment needed to hold and maintain the cryogenic temperatures is very heavy. For a sample return mission, Ash, et. al., found the power required to keep the hydrogen liquid would be about 1000 W.[3] The increased power and storage requirements have been found to take up any mass saved by the ISRU production of propellants.

SOE technologies have been around for some time, and the idea of using them for space exploration did not actually originate with Ash, et.al.. In the 1960's extensive work was done on SOE systems for O_2 reclamation on long manned space flights. Most of the work in this area has been done by Westinghouse, starting in the early 60's and continuing into the 80's. Eliken, Archer, and Zahradnik stated the problem: "As space missions become longer than about a month, the possibilities of generating oxygen in situ become

attractive because of the difficulty and expense of continued resupply from Earth."[12] Several studies have shown solid oxide electrolysis was a promising technology for converting waste CO_2 to oxygen.[13,13,14,15,16] Weissbart, Smart, and Wydeven at Ames noted SOE systems did not have any gas-liquid phase separation problems in microgravity environments.[16] Westinghouse went as far as building a breadboard system capable of supporting three people.[17] The work in ISRU for propellant production builds on the history of SOE research in life support, and in fuel cells.

BASIC ELECTROLYSIS

The Electrolyte

The central idea behind the entire solid oxide electrolysis technology is a number of oxides are capable of transporting oxygen ions. Zirconia is one of these oxides, and will be used to illustrate the concept.

In crystalline form, Zirconia (ZrO_2) is a polymorph. Pure ZrO_2 has three different structures: cubic, tetragonal. and monoclinic, as seen in Figure 3. The cubic phase has the best ion transport properties. Unfortunately, this phase is only stable between 2370 and 2680 °C.[18] By adding dopants, such as CaO, MgO, Y_2O_3, Sc_2O_3, and others, the cubic structure can be stabilized, allowing it to exist at temperatures as low as room temperature.

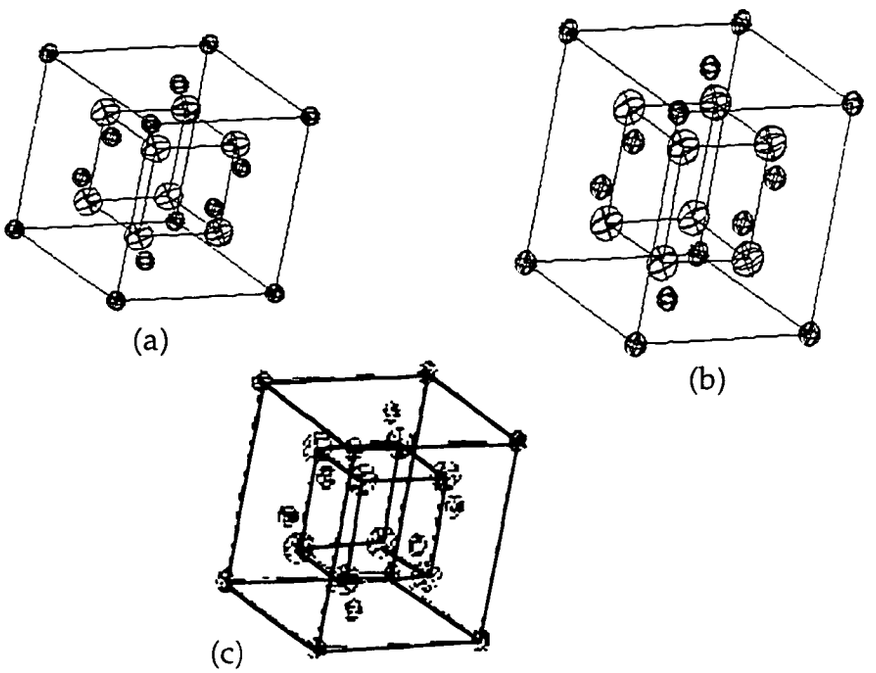

Figure 3. Polymorphs of Zirconia. (a) Cubic, (b) Tetragonal, (c) Monoclinic

The addition of a dopant compound has the added benefit of creating oxygen vacancies in the structure, which enhances the oxygen ion transport. Strickler and Carlson found the oxygen conductivity of zirconia increased as the size of the dopant cation decreased. They attributed this effect to an increase in ionic mobility with the smaller cations.[19] Scandia was the only dopant they studied with a cation smaller than zirconia. The conductivity of scandia doped zirconia was found to be more than two times greater than yttria stabilized zirconia: 25.4 $\Omega^{-1}m^{-1}$ for 10% Sc_2O_3, and 11.62 $\Omega^{-1}m^{-1}$ for 10% Y_2O_3, at 1000 °C.[19] However, scandia doped zirconia is not commonly available. Yttria stabilized zirconia, on the other hand, is used in many electronics applications, and is readily obtained. Therefore, most research, including this study, is done using yttria.

The doping process can be described using Kroger-Vink notation.

$$Y_2O_3 \xrightarrow{2ZrO_2} 2Y'_{Zr} + 3O_O^x + V_O^{\bullet\bullet} \qquad (1)$$

A mole of yttria replaces two moles of zirconia. Two moles of yttrium sit on two moles of zirconia sites. The three moles of oxygen added to the structure sit on oxygen sites. The difference in valance between the cations requires one mole of oxygen vacancies be added for every mole of yttria added to the ceramic.

The benefits of adding dopants does not extend monotomically. For zirconia, there is a maximum in the ionic conductivity at about 8-9% yttria. After this point, the conductivity decreases, due to defect association.[18] As the number of defects increases, there is a greater chance they will cluster together, balancing out any charge difference, which increases the activation energy needed for an ion to move onto the site.[20,21] Strickler and Carlson also suggest a second phase may form at this point.[19]

The process by which an ion travels through the electrolyte is relatively well understood. The notion of an atom actually passing through the material is misleading. An oxygen ion on the surface will find an oxygen vacancy also on the surface, and bind to it. At this point, the crystal has an excess negative charge. Oxygen ions shift throughout the crystal in an attempt to balance its charge. When these shifts reach the opposite side of the electrolyte, an ion will be kicked out of the crystal structure, restoring the charge balance. It has been found there is very little difference in conductivity between single crystal electrolytes and polycrystalline electrolytes. In addition, crystal orientation plays no role in determining the conductivity of zirconia electrolytes.[20]

The force that drives the ion shifts is an effect of both chemical and electrical potentials. The total potential of the process is given by the equation

$$\eta_i = \mu_i + z_i F \phi \qquad (2)$$

where μ_I is the chemical potential, z_i is the effective charge, F is Faraday's constant, and ϕ is the electrical potential.[18]

The reactions that take place on the surface are strongly dependent on the partial pressure of oxygen at the surface.[18] The local defect concentration can change with pressure, so the surface structure will also change with pressure. At a certain point, oxygen vacancies will cease to be the dominant defect, and electronic conduction will ensue. Fortunately, the ionic conductivity of zirconia stays constant and dominant over a wide range of pressures (1 atm to 10^{-20} atm, at a minimum)[22], but a difference in the oxygen pressure on opposite sides of the electrolyte will cause a drop in voltage across the cell, as the ceramic attempts to maintain a charge balance.

This voltage drop was quantified by Nernst around the turn of the century. The voltage drop is actually a function of equilibrium constants, but it is usually given in terms of the pressure,

$$\Delta\phi = \frac{RT}{4F} \ln\left(\frac{P_{O_2}^a}{P_{O_2}^b}\right) \qquad (3)$$

where R is the gas constant, T the temperature, F Faraday's constant, and P_{O2}^i the partial pressure of oxygen on side a and b of the electrolyte.[18] This voltage occurs whenever there is a difference in oxygen pressures across the ceramic. When used as a fuel cell, this voltage is the voltage of the cell. Since the voltage is proportional to oxygen pressure, a zirconia cell can also be used as an oxygen sensor.

If the cell is being run as an electrolysis cell, the Nernst voltage becomes a loss. In almost all cases, the electrolysis process forces oxygen ions to go from the low pressure side to the high pressure side of the cell. A voltage must be applied to force the oxygen ions through, which means it must be higher than the Nernst potential. Unfortunately, it is hard to know what the oxygen pressure at the crystal is, since it is affected by the structure of the electrode, as we will see later.

If too high a voltage is applied to the cell, oxygen ions will be driven from the crystal structure itself. For zirconia, this voltage has been found to be about 2.23 volts.[10] In cases where the oxygen pressure is very low, this can drop to as low as 1.4 volts.[17] There are two effects of the cell breakdown. The most obvious one is the cell starts to develop microcracks, and eventually the ceramic can no longer hold itself together. A less intuitive effect is the onset of electronic conduction. As the electrolyte is reduced, the n-type conductivity increases,

increasing the current through the cell.[22] The increase in current is a sign that breakdown is occurring, and the cell has ceased to function.[4]

A zirconia cell can be damaged by too much current. This condition results in the blackening of the electrolyte. This visible change of color indicates the start of electronic conduction.[23] The electrolyte resistance increases as well. There is some indication the black color is due to the formation of zirconium particles in the electrolyte as electrons fill anion vacancies.[23] In CO_2 atmospheres, blackening does not occur until the voltage across the cell reaches about 3 volts, at temperatures of about 1380 °C.[23] It should not play a role in this research.

Of course, for the oxygen to be transported through the ceramic at all, it, as well as the current, must first get there. That is the job of the electrode.

The Electrode

The zirconia electrolyte resistance is fairly well understood. The resistance associated with the oxygen ionic conductance is a simple ohmic resistance.[24] It can be modeled fairly simply. Unfortunately, the electrode reactions do not share this characteristic. They are dependent on many factors, such as oxygen partial pressure, temperature, flow rate, electrode structure, and the applied voltage.[25,26]

Klietz defines an electrode as the interface between an electronic conductor and an ionic conductor.[27] This definition is different from the everyday use of the term electrode, which would include, in our case, the entire platinum film, not just the interface. Most researchers use the term in the everyday sense. Many of the electrode processes can be understood in terms of the surface structure and surface energy. Unfortunately, while many electrolytes have simple surfaces, the electrodes often do not.[28] In a real world situation it is impossible

to know the details of a sample surface, and therefore pointless to try to explain things in terms of the surface energy.

Blakely has shown that ionic conductors are mathematically analogous to semiconductors, allowing the electrodes (in the strict technical sense) to be described with Fermi diagrams.[29,30] Figure 4 shows an energy level representation of an electronic conductor, an ionic conductor, and an interface between the two. As the diagram shows, the electrode forces the ionic and electronic conduction levels to meet. "The Fermi level gradient results in a micro electronic current which is compensated by an equivalent microionic current. This is the so-called electrochemical semi-permeability phenomenon."[27] In all electrode/electrolyte combinations, one type of conduction will dominate. For a Pt electrode with a ZrO_2 electrolyte, the electronic link dominates.

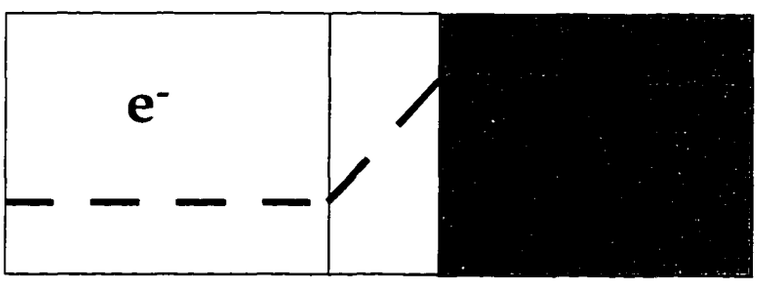

Figure 4. Energy Level Diagram at the Interface of an Electrical and an Ionic Conductor.

Since the electrolyte resistance is a simple ohmic resistance, the existence of limiting currents and decay of cell voltages "indicates that a kinetic or configurational hindrance of the electrochemical reactions is taking place at one or both electrode-electrolyte boundaries."[25] This hindrance is the electrode resistance. The above statement makes a very important point by the way it is worded. Many electrodes have a layer of charged particles on each side of the

interface. These particles form a capacitor, which is called the double-layer. However, this is not entirely the case in Pt/ZrO_2 interfaces. The capacitance in this electrode is much higher than a double layer can account for. Both the resistance and capacitance effects in the Pt/ZrO_2 system are chemical effects, not electrical ones.[29]

The overall chemical reaction for oxygen production is[27]

$$\mathbf{CO_2\ (g) + 2e^-\ (Pt) + V_o^{\bullet\bullet}\ (ZrO_2) \rightarrow CO\ (g) + O_o^x(ZrO_2).} \quad (4)$$

Most studies are done with pure oxygen as the reactant gas. All of the studies reviewed here are based on the following reaction.[26]

$$\mathbf{1/2\ O_2(g) + V_o^{\bullet\bullet}(ZrO_2) + 2e^-(Pt) \rightarrow O_o^x(ZrO_2).} \quad (5)$$

Both these reactions use elements from the gas, electrode, and electrolyte. This requirement means the reaction must take place in a region near the triple boundary between the gas, electrode, and electrolyte.[26] Pizzini lists the steps that could occur during the electrode reaction.

- $V_o^{\bullet\bullet}$ diffusion in ZrO_2
- O_2 diffusion in gas phase
- O_2 diffusion in pores
- Oxygen chemisorption and dissociation on Pt surface
- Oxygen diffusion on Pt surface
- Oxygen diffusion at Pt grain boundaries
- Diffusion of oxygen into Pt
- Oxygen chemisorption, dissociation, and diffusion into ZrO_2
- Dissolution and diffusion of oxygen in ZrO_2
- Electron migration into ZrO_2
- Electrochemical reaction of electron transfer at the boundary.[25]

The key area of research in the field of electrode/electrolyte interactions is the determination of the rate determining step.

The one point of agreement between all studies is the existence of a strong inconsistency between results. The explanation of the discrepancies is also agreed upon. The electrode reactions are dependent on so many things, it is difficult to separate out the effect being studied. All of the following are known to affect electrode reactions.[24,25,26,31,32,33]

- Preparation method
- Material
- Electrode history
- Electrode shape
- Electrode structure
- Applied Voltage
- Temperature
- Pressure

One of the keys to studying the electrode/electrolyte interface is the careful preparation of the sample. Without care, the results will never be reproducable.[25,32,33] The electrolyte surface should be polished, and care must be taken to achieve a good, even, clear interface between the electrolyte and electrode material.[33]

Electrode materials are very important. The limiting current densities in one experiment ran from 0.03 mA/cm^2 for gold to 21 mA/cm^2 for rhodium.[34] It turns out, however, the reaction is much less sensitive to the electrolyte dopant. In fact, there is no difference in results for zirconia if it is doped with 8-21 mole % yttria, or 11 mole % calcia.[35]

The annealing process has a large effect on the electrode resistance. On one hand, by annealing at high temperatures, carbon deposits can be removed from the surface. These deposits compete with the oxygen for reaction sites, so

a large amount of carbon contamination can reduce the reaction rate of the oxygen.[32] On the other hand, the annealing process lowers the number of active sites, thereby raising the electrode resistance. However, these cells operate at high temperatures, so they will anneal anyway. It is therefore desirable to anneal the cell at a higher temperature than the operating temperature, to eliminate structure changes during operation.[25]

Porosity is a very important factor in determining the cathodic reaction rate. Many electrode depositing techniques create non-porous electrodes. Both paste and sputtering techniques can produce non-porous electrodes.[24,33] Bauerle suggested non-porous electrodes can be made artificially porous by passing a heavy current through the electrode. He used 1 A/cm^2 at 800 °C. His explanation for the effect is the heavy current produced pockets of oxygen at high pressure at the interface. These pockets then burst, creating pores through the electrode.[24] The porosity lowered the electrode resistance.[24] Pizzini, et al. had similar results. They also found the resistance decreased after what they call anodic heavy current treatment. They applied the current during the annealing process. The benefits, according to Pizzini, do not come from bursting high pressure gas pores, but instead come from enhanced sintering. The "anodic treatment...seems to play an important role in determining the interfacial tension at the Pt/electrolyte contact."[32] The sintering process is controlled by the surface tension. The heavy current treatment results in both increased Pt grain size and pore size, as well as improved surface adhesion.[25,32] Gur, et al., noticed a difficulty in using the heavy current treatment. The shock of the treatment can break the electrolyte disk, as well as blacken the cathode side of the ZrO_2, allowing electronic conduction.[33] They arrived at a simple solution: "Cycling the...cell between 0

and 2 V at the highest working temperature using small voltage increments until no hysteresis is observed."[26] The hysteresis in the I-V plot indicates significant morphological changes are occurring. Gur agrees with Bauerle on the mechanism of pore production.[33] Since Pizzini applied the current during the sintering process, as opposed to afterward, any gas pockets that formed would affect the surface energy, increasing the pore size through sintering instead of bursting through the hard and solid already sintered electrode.

If the electrode becomes too porous, resistance can be impeded by constriction resistance. When only part of the surface is involved in the reaction, local spots of high current density can appear, which can cause the apparent resistance to increase, as well as the real resistance, through morphology changes.[25,33]

There is little agreement on the rate determining step. The determination of which step is the rate determining step is done by comparing oxygen partial pressure dependencies and activation energies with known processes. For example, if the P_{O2} dependence is linear, the rate determining process involves molecular oxygen, if there is a square root dependence the process involves atomic oxygen.[25] Unfortunately, there isn't even agreement on the partial pressure dependence.[26]

Pizzini has found the rate limiting step is dependent on temperature. At low temperatures, the rate limiting step is oxygen surface diffusion.[32] He arrives at this conclusion through elimination. His data shows a square root dependence. All steps involving molecular diffusion are therefore eliminated. All electrolyte processes are ruled out by observing that the rate is dependent on electrode material. The electrochemical reaction can't be rate limiting because the anode

electrode doesn't suffer from any 'hindering'.[25,32] Finally, the oxygen diffusion rate in Pt is very slow. This leaves surface diffusion as the rate limiting step. At high temperatures, he found the rate determining step is not an activated process, indicating the rate is limited by the desorption of chemisorbed oxygen.[25,32] Klietz also has found that adsorption plays an important role.[29] Isaacs, et al, are somewhat in agreement, finding the rate is limited by adsorption of oxygen on the electrode surface.[34] Their study was carried out at high temperatures.

Gur has found a linear P_{O2} dependence for the reaction. He concludes the rate limiting step is boundary layer diffusion in the gas phase.[26] The major difference between his work and Pizzini's is the pore size in the electrode. Gur's electrodes had pores about 1 micron in diameter, where Pizzini had pores up to 6 microns. The smaller pores could be constricting the diffusion of O_2 molecules through the electrode. Pizzini suggests this in his later paper.[25]

Gur and Huggins have also found the rate is dependent on the applied overvoltage. At low voltages, the polarization related to slow diffusion of oxygen on Pt controls the rate. At high voltages, the I-V characteristics are nearly reversible. At temperatures over 800°C, they found the process dominated by the resistance of the electrolyte.[33]

There is another school of thought, led by Kroger and Brook. Brook interprets the data to indicate the rate limiting step is either the diffusion of atomic oxygen through Pt (low voltage), or the diffusion of adsorbed oxygen to F-centers in the zirconia electrolyte, where it combines with electrons traveling into the electrolyte.[36]

Mizusaki, Amano, Yamauchi, and Fueki offer equations that predict the conductivity of an electrode. Their findings are almost the reverse of Pizzini's.

They find surface diffusion to be the rate limiting step at high temperatures, and the "dissociative adsorption of oxygen molecules on the Pt surface near the Pt/zirconia boundary" to be limiting at low temperatures.[35] The electrode conductivity is given by[35]

$$\sigma_e = \frac{4F^2 Bc\lambda a_o^{\bullet} P_{O2}^{\frac{1}{2}}}{\delta\left(a_o^{\bullet} + P_{O2}^{\frac{1}{2}}\right)^2} \qquad (6)$$

for high temperatures, and

$$\sigma_e = \frac{16FAka_o^{\bullet 2}}{RT} \qquad (7)$$

for low temperatures. B is the triple boundary length, c is the adsorption site concentration, λ a constant related to the surface mobility of adsorbed oxygen atoms, a_o is the oxygen activity, δ is the average diffusion length, and ka_o^2 is the rate constant for the adsorption process.[35] Both these processes are occurring at all temperatures, but the first equation is dominate at high temperatures, and the second is dominate in cooler regions.[35] The difficulty with their interpretation is it assumes the adsorption process is not pressure dependent, which seems unlikely.

Klietz also talks about the reaction during the mixed conduction region of zirconia. This region is noted by a sudden decrease in electrode resistance, as electrons are allowed into the electrolyte.[29]

There does not appear to be any clear winner in the debate at this time. The interpretation given by Pizzini, et al., is the most appealing. They carefully go through the process that led them to their conclusions. The other papers gave a more cursory interpretation. However, since it is difficult to control the preparation process completely, an individual cell might show results inconsistent with this theory. At this point, it is still necessary to examine each cell and processing combination and make independent determinations.

Combined Models

Many researchers in the ISRU field try to avoid the difficulties of the electrochemistry by combining the electrode effects with the Nernst potential, creating a modified Nernst potential that gives the voltage required to transport oxygen.

One attempt was by Ash, Dowler, Hanson and Uphoff. They derived the following equation

$$\Delta\phi = kT \ln\left[\frac{P_2 + \Delta P_e}{x_{O_2} P_1 - \Delta P_e}\right] E_i j (R_s + \rho t) \qquad (8)$$

where ΔP_e is the pressure drop across the electrode, x_{O2} is the oxygen percentage on the input side of the cell, P_1 is the input pressure, P_2 is the output pressure, E_i is the ionization overpotential, j is the current density, R_s is the surface resistance, ρ is the electrolyte resistance, and t is the thickness.[5] This relationship is still difficult to work with. The ionization overpotential and the surface resistance of the electrode are hard to determine, and almost impossible to plan in advance. An earlier relationship derived by Richter is slightly more

usable

$$\Delta\phi = \frac{RT}{zF} \ln\left[\frac{P_2}{\left(\frac{K(1-n)}{n}\right)^2}\right] \qquad (9)$$

$$n = c\left(\frac{I}{\dot{m}_{CO_2}}\right) \qquad (10)$$

where K is the equilibrium constant of the carbon dioxide dissociation reaction, and c is a constant determined experimentally to be 6.969.[37] This expression reaches limits when either there is no impedance to oxygen flow on the carbon dioxide side, or when the pressure drop across the electrode is equal to the pressure on the CO_2 side, and the current is 0.[4]

Others have used expressions based on the voltage applied to the electrolysis cell. Erstfeld and Mullins used a very simple equation

$$I = \Delta E \sigma \frac{A}{l}, \qquad (11)$$

where ΔE is the difference between the applied voltage and the required voltage, and σ is the conductivity of the system.[38] The required voltage can be found by using the equations mentioned previously.

All these equations were successful for the systems on which they were developed. They have a tendency to break down when applied to other systems. As mentioned in the previous section, there are many factors which influence the electrochemical processes, which can not be accounted for in these equations. Differences in temperature, pressure, and electrode structure can greatly alter the results, as they can change which mechanism dominates the process.[39]

PROJECT GOALS

The University of Arizona has been investigating solid oxide electrolysis as an ISRU technology since 1985. Several systems and geometries have been tested, in both single and multiple cell configurations. The primary areas of concern in these tests were the electrolyte performance and the scalability of the systems.

In the summer of 1994, it became apparent the electrode played a crucial role in the performance of the system. At the time, electrodes had primarily been applied by handpainting electrodes onto the zirconia disk or tube. Very little care was given to the reproducibility of the results. Not surprisingly, there was a large spread between data from different systems. It was not possible to control the thickness of a handpainted electrode, nor was it possible to guarantee an even coating. As a result, it was not possible to determine the effects the electrode had on the system performance. The MiniMOX project was designed to determine those effects.

There are two major goals in this project. The first was to develop a system to test the electrolysis cells. The system had to be flexible enough to allow both the easy changeout of samples, and the collection of any data required. It also had to be reusable. Previous systems had ceramic seals that failed after one temperature cycle. The new system was designed to use metal seals, which could be taken apart, and then put back together again with a minimum of work. The new system also required the use of computer data acquisition, to allow the system to run and collect data for long periods of time without

supervision. Finally, the system had to be able to supply a number of gases to the cell as feedstock: Ar, O_2, CO_2, and a Mars atmosphere simulant.

The other major goal was the examination of the electrode. Different electrode configurations were to be tested. The results would be used to design the electrodes for MOXCE, a 16 cell full scale prototype of an oxygen production system for use on a Mars Sample Return mission. The MOXCE project also gave this project its name. As a single cell version of MOXCE, this project's name became MiniMOX. The electrodes were to be carefully prepared, so results could be reproduced. At the end of the MiniMOX project, there should be enough data to confidently predict MOXCE's output.

This thesis covers the development of MOXCE, and the preliminary results from the electrode tests. Four electrodes were examined for this thesis. Two were prepared from the electrode paint used on previous systems, and two were coated using an evaporative deposition technique to a thickness of 0.5 microns. The data obtained was in the form of current vs. voltage curves, and current vs. time.

THE MINIMOX SYSTEM

MiniMOX

The heart of the prototype test system is MiniMOX itself. This subsystem consists of two platinum plates with three platinum tubes attached to it. These plates hold the electrode/electrolyte sandwich in place, and provide the current for the electrolysis process. The tubes are for the gas inlet and outlets.

The system had to be reusable, so ceramics could not be used. Past experience with ceramics has shown they develop cracks after only a few temperature cycles. Some of the systems show cracks after one cycle. Since the system has to run at high temperatures, in an oxygen atmosphere, our choice in materials were limited.

Platinum was selected as the material for MiniMOX based on material compatibility. The coefficient of thermal expansion of platinum is almost identical to that of zirconia, both being about 10^{-5} $°C^{-1}$. Therefore, both the electrolyte and its holder will expand at the same rate as the system is heated. In addition, platinum does not bond with zirconia all that easily. Nickel, another high temperature material, forms a low melting point eutectic with zirconia. We placed a zirconia crystal sandwiched between two nickel plates in an oven, and heated them to 1000 °C. The nickel reacted with the zirconia, forming a tight bond. Upon cooling the two materials contracted at different rates, causing the zirconia to cleave down its long axis. Figure 5 shows the remains of the crystal.

The restriction of materials to metals, and the thermal and chemical characteristics involved, forced us to make the uneconomical choice of platinum as the material for MiniMOX.

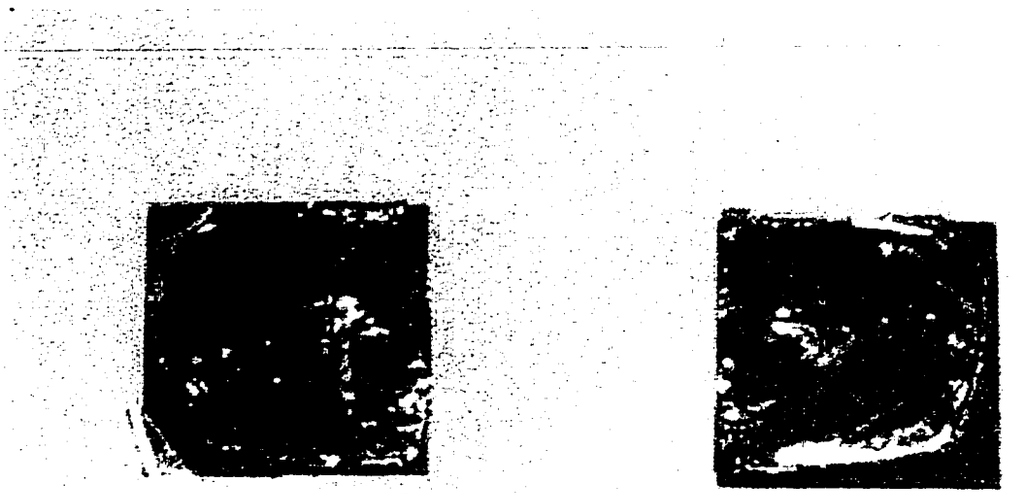

Figure 5. Crystal Cleaved by an Interaction with Nickel.

As stated above, MiniMOX consists of two plates. The plates were designed by Dr. Steve Crow. The lower plate is the input side. Two tubes are attached to this side. One tube is for the input gas, and the other is for the waste gas. The plate itself is triangular, with a raised ring to contact the electrode on the electrolyte disk. The dimensions are shown in Figure 6.

The top plate is identical to the bottom one, except there is only one tube leading from it. This tube is for oxygen to be removed from the system. Figure 7 shows the top plate. The diagram of the entire system is shown in Figure 8. Photographs of the system, both assembled and disassembled, are provided in Figures 9 and 10.

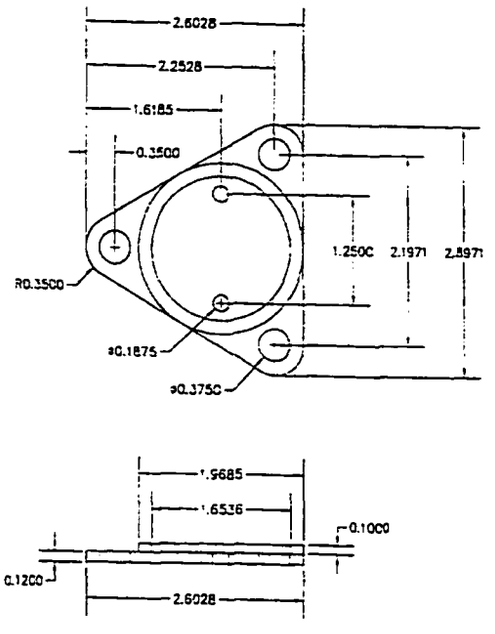

Figure 6. MiniMOX Bottom Plate. (Drawing by Steve Crow)

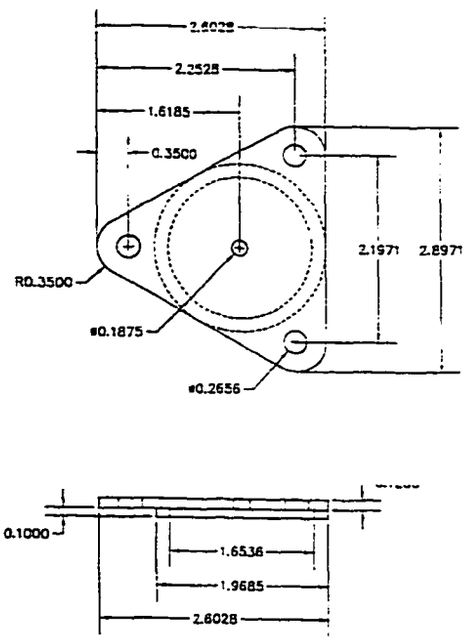

Figure 7. MiniMOX Top Plate. (Drawing by Steve Crow)

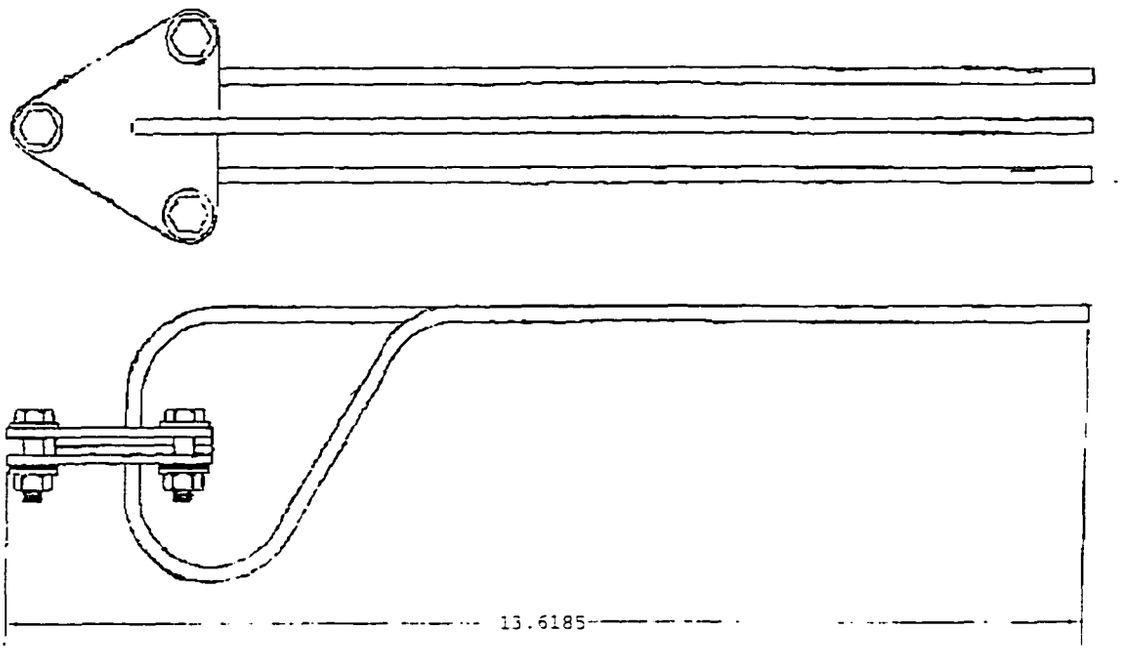

Figure 8. Assembled View of MiniMOX. (Drawing by Steve Crow)

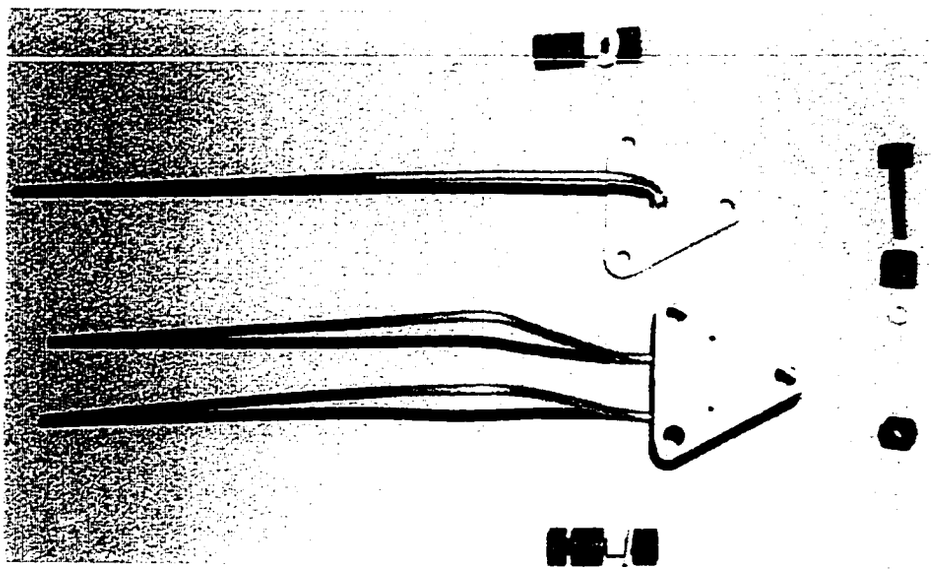

Figure 9. Disassembled View of MiniMOX.

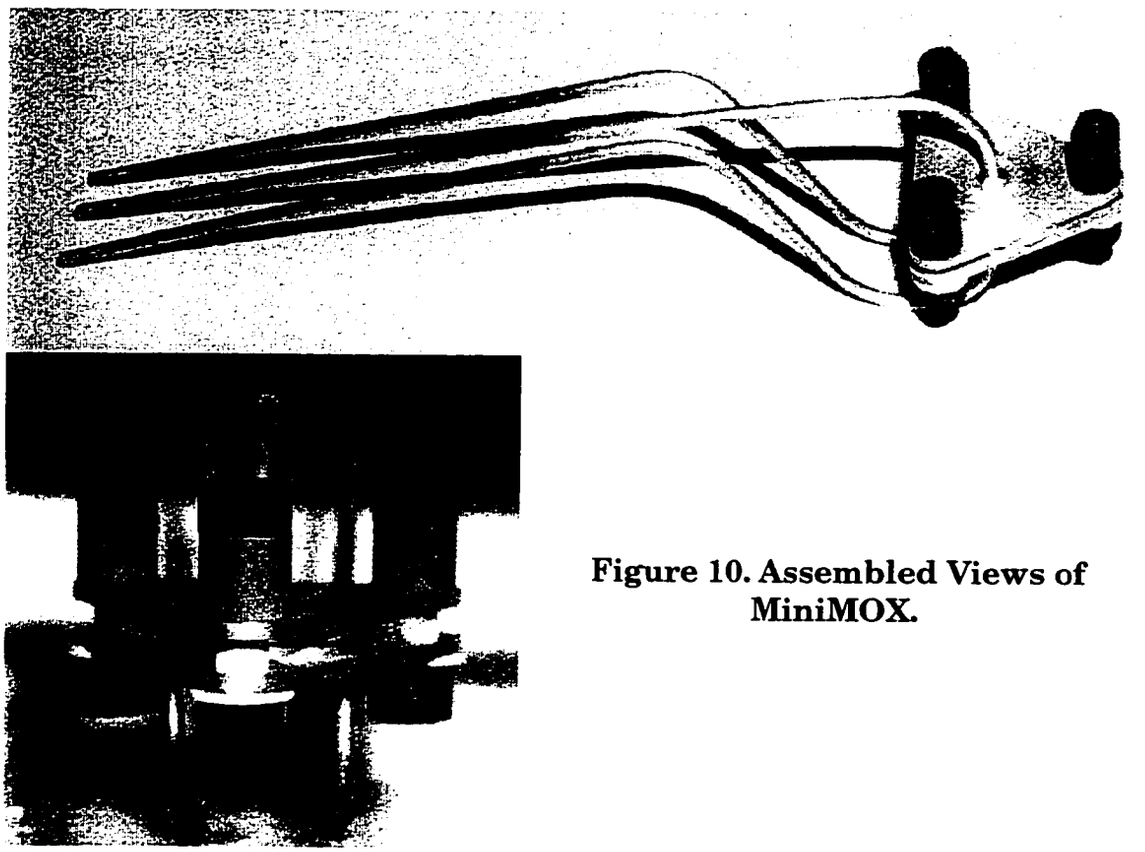

Figure 10. Assembled Views of MiniMOX.

Sealing has long proven to be a difficult issue in these systems. Much of the difficulty is from the need to disassemble the system. The fuel cell industry would simply seal the system with a high temperature glass. Unfortunately, such a seal can not be removed. Since the cell can be characterized entirely from voltage-current plots, the decision was made to accept a small amount of leakage in and out of the system. The rings on the plates were originally polished to within five microns of flat. They have since been allowed to roughen through use. Even in their roughened state, the leak rate on the input side is often less than 5% of the input flowrate, depending on the disk being used. Often it is down to about 2%.

Bolts

Another difficulty caused by the need to take MiniMOX apart was finding a way to hold it together at high temperature that would allow the system to be disassembled when cool. The first method attempted was the use of platinum bolts. The bolts would expand along with the system to preserve tightness, but the high temperature softened the threads to the point where the nut could not be removed after two temperature cycles.

The problem was solved with the design of bimetallic bolts. The bolt itself, along with the nut, was made from Inconel 758 This material has an expansion coefficient of 1.4×10^{-5}, 40% higher than platinum and zirconia. As the temperature increased, this bolt would become loose. A spacer was added, made of Hanes 214, which has an expansion coefficient of 1.8×10^{-5}. The spacer would expand faster than the bolt, holding the system to the desired tightness. Both Hanes 214 and Inconel 758 are very oxygen resistant. They retain much of their conductivity in oxygen rich environments at high temperatures. To prevent

an electrical short, a zirconia sleeve is inserted around the bolt at the bottom plate, and a ceramic washer separates the nut and the bottom plate. Figure 11 is a diagram of the bolt system, and Figure 12 is a photo of the bolt system. These bolts have proven to hold up to the high temperature environment with no evidence of decay.

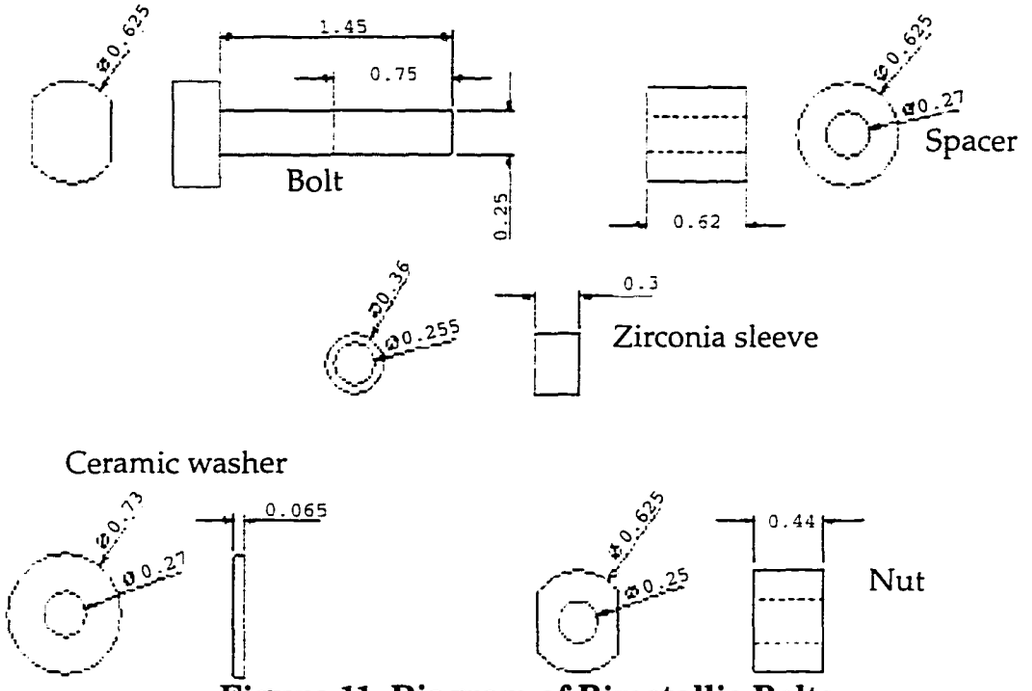

Figure 11. Diagram of Bimetallic Bolts.

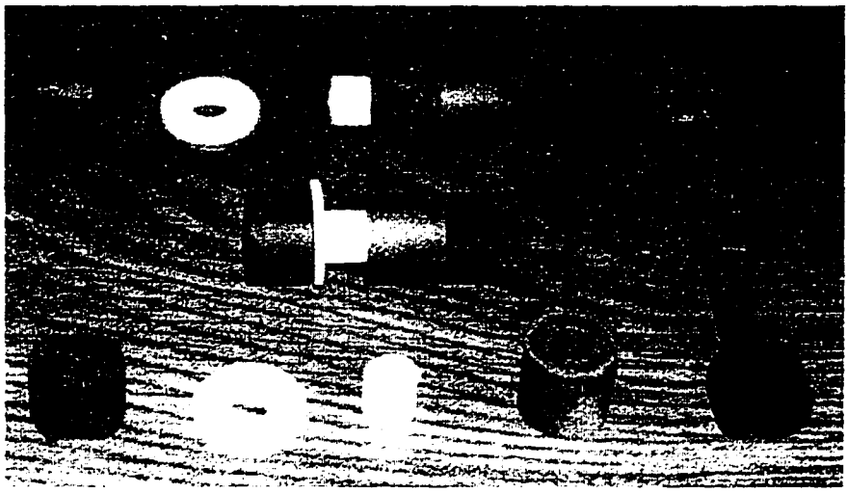

Figure 12. Bimetallic Bolts.

Oven

An oven is required to heat MiniMOX to the required temperature of 1000 °C, and maintain that temperature. The Lindberg/Blue M Model 51848 was chosen for this task. This oven was modified by adding three holes in the back to allow the platinum tubes from MiniMOX to exit the oven. The dimensions of the interior of the oven are 4" x 4" x 8".

The oven has an electronic controller that allows two ramps, two dwells, and two temperatures to be set. The controller can also be connected to a computer through an RS-232 port to allow computer control.

The maximum rated temperature for the oven is 1100 °C. Figure 13 shows photos of the front and back of the oven. Note the holes for MiniMOX in the back.

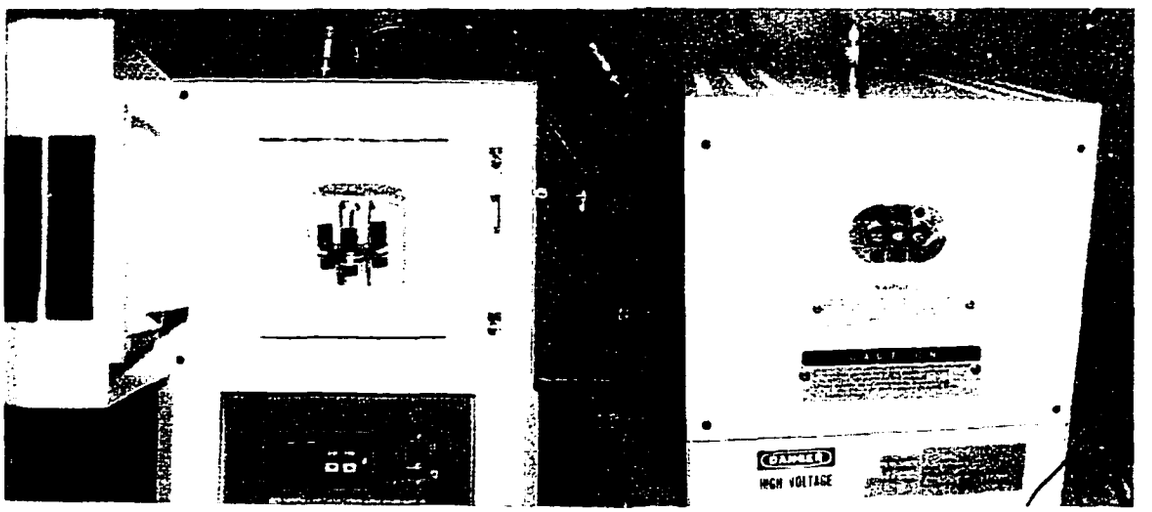

Figure 13. Front and Back Views of the Blue M Oven. MiniMOX can be seen in the front view.

Power System

Power is supplied to the cell through the gas line connections. Screws were welded to the swagelock T-connectors, and leads from the power supply attached to them, as shown in Figure 14. The metal T-connectors are attached to the platinum tubes. When properly tightened, this arrangement provides a solid connection.

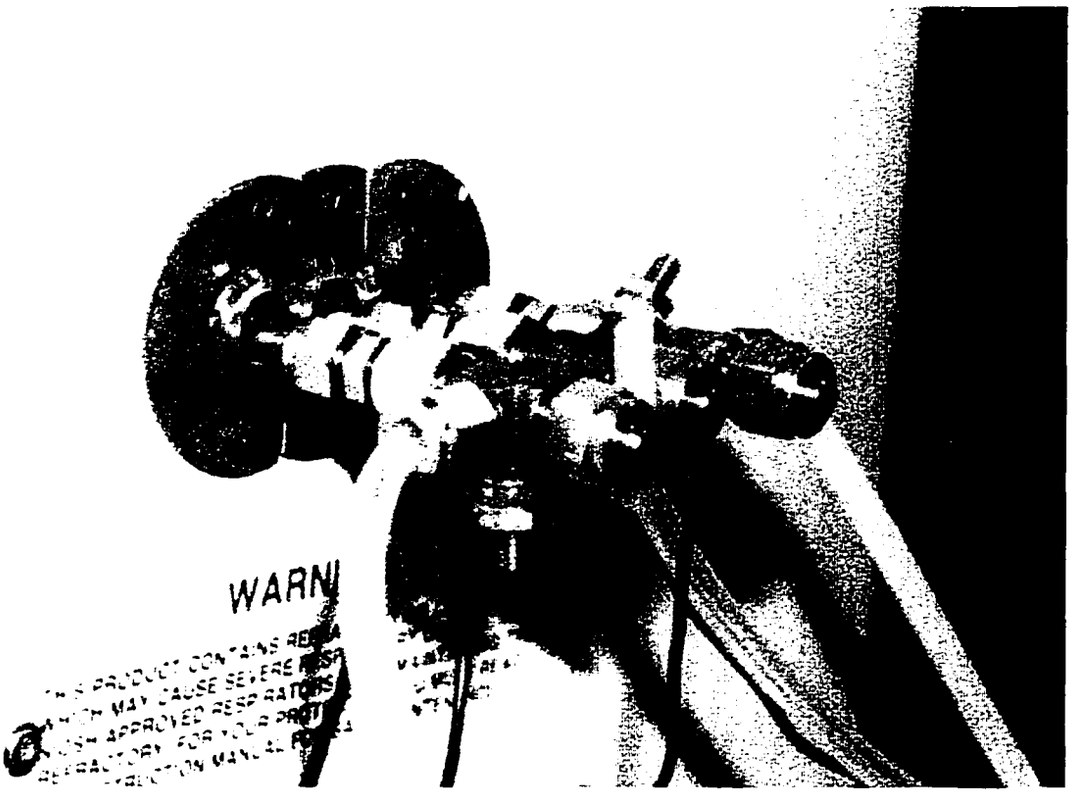

Figure 14. Power and Gas Connections for MiniMOX.

The main power from the cell comes from a Acopian PO6HX1600 DC power supply. It maintains a set voltage level chosen by the user from screws on the front panel. Figure 15 shows the DC power system. The negative lead of the power supply is attached to an American Alliance digital display set to

measure the current. The lead from the current meter is attached to the input side of the cell through the swagelock T-connector. The positive lead runs from the power supply to the current input of the signal conditioner, and from there to the output side of the cell.

There is also an American Alliance display attached to the sensor outputs of the power supply. This display shows the voltage applied to the cell. The actual total voltage of the cell is measured by the data acquisition system through leads attached to the T-connectors.

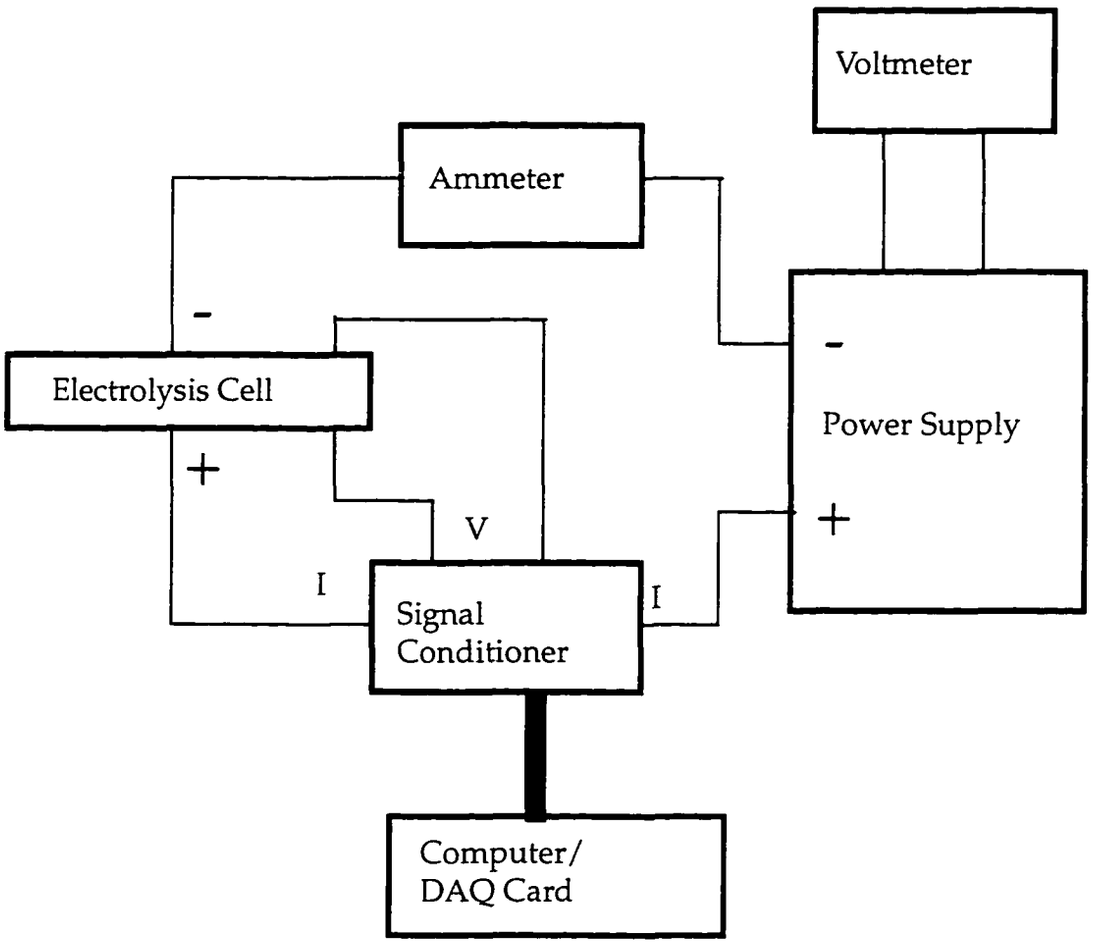

Figure 15. DC Power System.

Gas Supply

The gas supply system provides a variety of gases to the system at a desired flowrate. The feed side of the system is hooked up to four gas bottles, as shown in Figure 16. The gases are argon, carbon dioxide, oxygen, and a Mars atmosphere simulant consisting of 95% CO_2, 3% N_2, and 2% Ar. Lines leading from each bottle are passed through Alltech gas purifiers, and are connected to the main valve panel. This panel allows the user to select which gas should be fed to the system. The output from the valve panel goes to an MKS flow controller, which allows the flowrate to be set precisely. Gas from the flowmeter runs past a pressure transducer and into the cell.

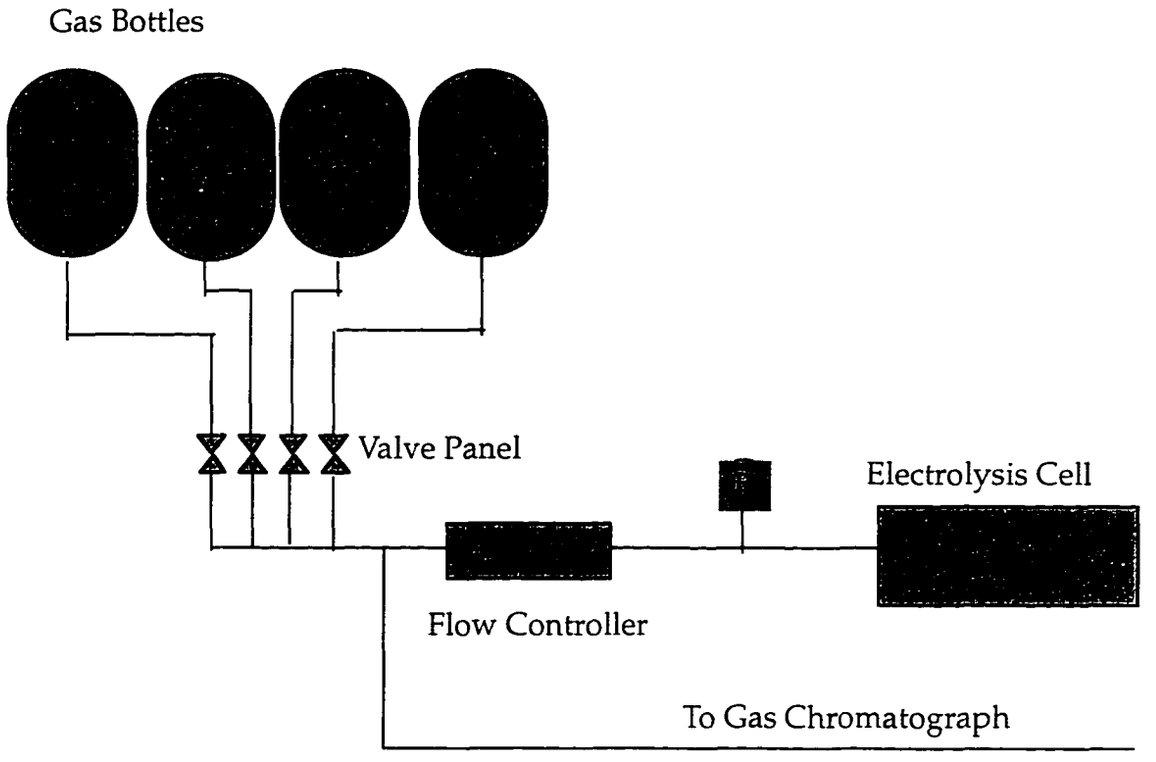

Figure 16. Gas Feed System.

Gas leaves the cell from two points. The waste line runs through a flowmeter, and then can be directed to an exhaust port, or towards a gas chromatograph. Gas from the oxygen side goes past a pressure transducer, through a flowmeter, and over to the gas chromatograph (GC). Another valve panel is located by the GC to allow the selection of the gas to be sampled. The input line, waste line, and output line can all be sampled. Figure 17 shows the layout of the output gas system.

All lines are 1/4" Teflon, connected by swagelock connectors.

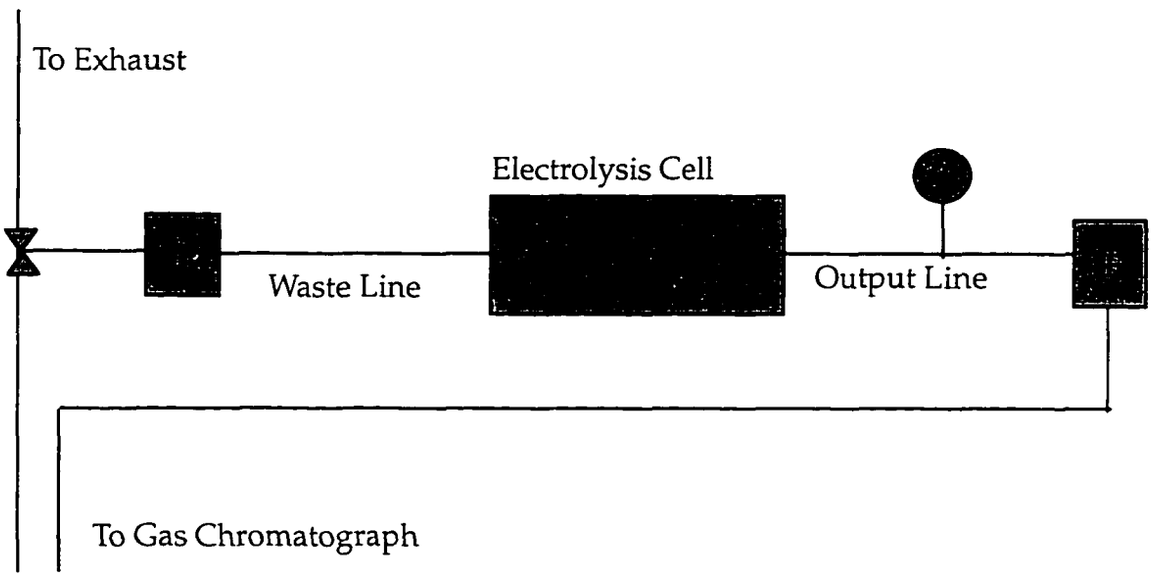

Figure 17. Gas Output System.

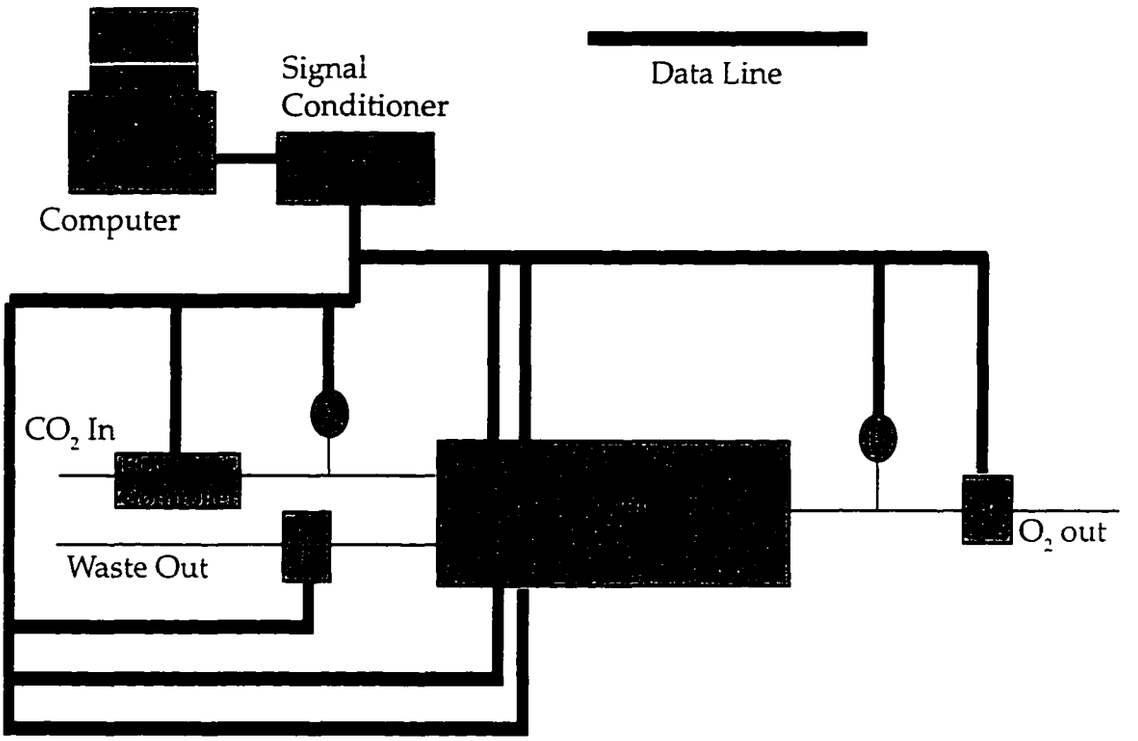

Figure 18. Data Acquisition System Schematic.

Data Acquisition System

The heart of the data acquisition system is a National Instruments DAQ-Card 700 PCMCIA data acquisition card. This card sits in the PCMCIA slot of a Zenith Z-Star 486 based Laptop computer, with 8 MB of RAM, a 230 MB hard drive, and a math coprocessor. The other end of the card is attached to a homemade signal conditioning box. This box amplifies the signals from the instruments to match the range of inputs the DAQ card is expecting. The signal conditioner can handle up to five thermocouples, three flowmeters, two pressure transducers, and one voltage and one current measurement. The current measurement is made by passing the current through a 0.1 Ω resistor. A diagram of the system is shown in Figure 18.

Two of the flow measurements are made from Omega flowmeters. The output line flowmeter has a range of 0-20 SCCM, and the waste line flowmeter has a range of 0-200 SCCM. The input flow measurement is from the MKS flowcontroller. All the flow instruments are powered with wall current.

The pressure transducers are currently 0-50 psi transducers from Omega that were inherited from earlier projects. Unfortunately, most of the pressure measurements desired are in the 0-2 psig range. The transducers we have do not produce accurate readings in this range.

The brain of the data acquisition system is the LabVIEW program written to control it. This program is called M-DACS, for MiniMOX - Data Acquisition and Control System. At the time of writing, the program is more advanced than the equipment it controls, so not all of its features are fully implemented.

M-DACS is designed to be capable of talking to oven controllers. This feature has been implemented for the Omega oven controller planned for use in MOXCE, but not for the Blue M oven being used for MiniMOX. The Blue M oven has a much more complicated protocol, and there has been no reason to automate this part of the system at this time.

M-DACS takes the voltage data given to it by the DAQ-Card 700 and converts it to the appropriate units. It then displays the units on the screen, as well as saving the data to a text file. Figure 19 shows the front panel for M-DACS. The program is also capable of calculating secondary results from the data, such as the power used by the cell. The user can set the frequency of the samples.

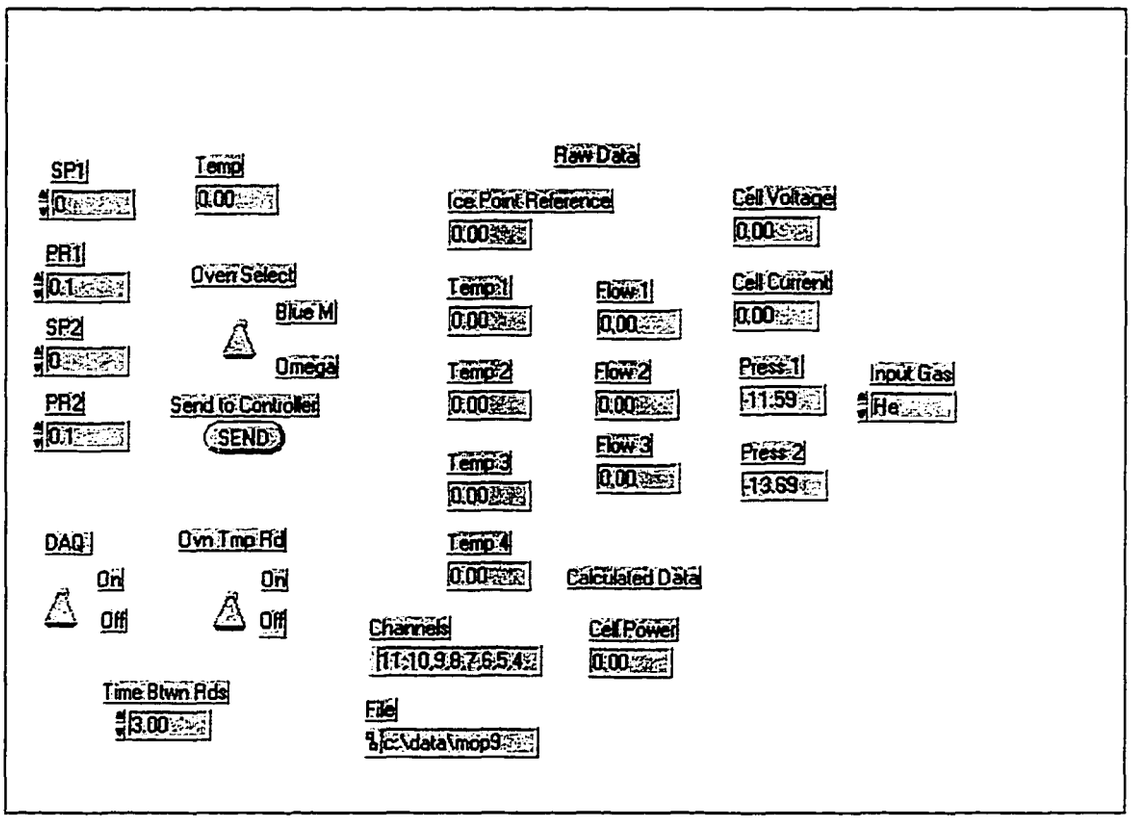

Figure 19. M-DACS Front Panel.

EXPERIMENT DESIGN, PREPARATION, AND EXPECTED RESULTS

Experiment Design

The objective of this series of experiments is to find the optimal electrode thickness and configuration for use on MOXCE. This thesis covers the initial set of experiments towards this objective.

The MiniMOX system described last chapter is designed to allow the study of several electrode/electrolyte samples in rapid succession. For this set of experiments, since the electrode was the object under study, all electrolytes were acquired from the same source. A single crystal zirconia disk, doped with 9.5% yittria was used. The crystals have a diameter of 50 mm and a thickness of 0.5 mm. All crystals were purchased from Zirmat Corporation. Dr. Steve Crow suggested the use of a single crystal to replace the polycrystalline electrolytes used previously.[40] A single crystal eliminates the resistance from the grain boundaries in a polycrystalline electrolyte. This reduction in resistance is not large, but an even more important benefit is the increased strength of the electrolyte. Polycrystalline zirconia disks are generally weak and prone to cracking, sometimes from just routine handling. The single crystals have survived short drops with no damage.

This first set of experiments is designed to demonstrate the loss in production with a very thin electrode. Four disks were prepared. Two were given a thick airbrushed coating, and two were given a thin evaporated coating of platinum.

The airbrushed electrodes were applied in house at SERC. A series of coatings of a platinum paint (Heraeus CL11-5100) were applied to the electrolyte. The disk was than heated to 1000 °C for two hours. The process was repeated until the coating had reached a thickness of 10-12 microns.

The resulting disks had a very uneven coating. Figure 20 shows the airbrushed coating. The circular imperfections were caused by thermal effects from the mounting method used during firing. The roughness of the surface does not seem to effect current flow, but does have a profound effect on the leak rate in the system.

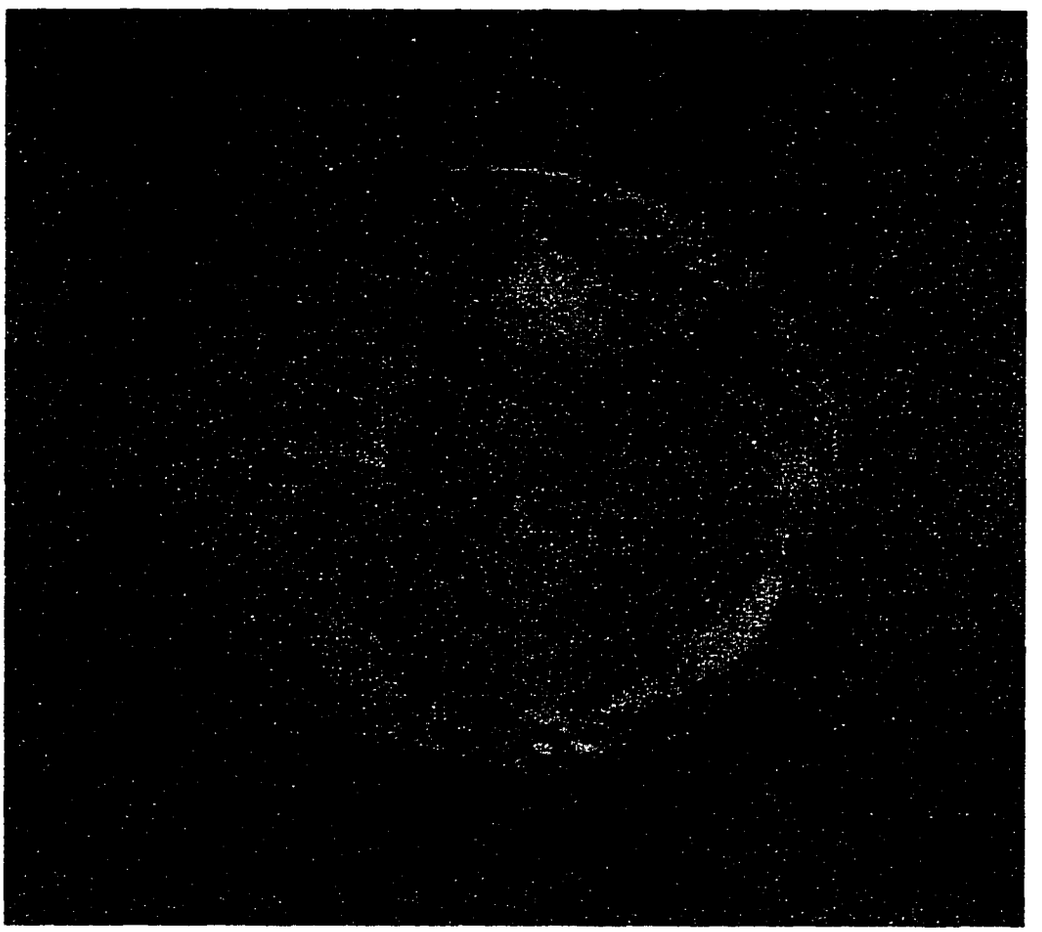

Figure 20. Airbrushed Electrode

When heated, the solvent in the platinum plate boils out, leaving a very porous spongy electrode structure, as shown in Figure 21. This structure allows gas to penetrate the electrode easily, while providing enough electrical connectivity to supply power to the process.

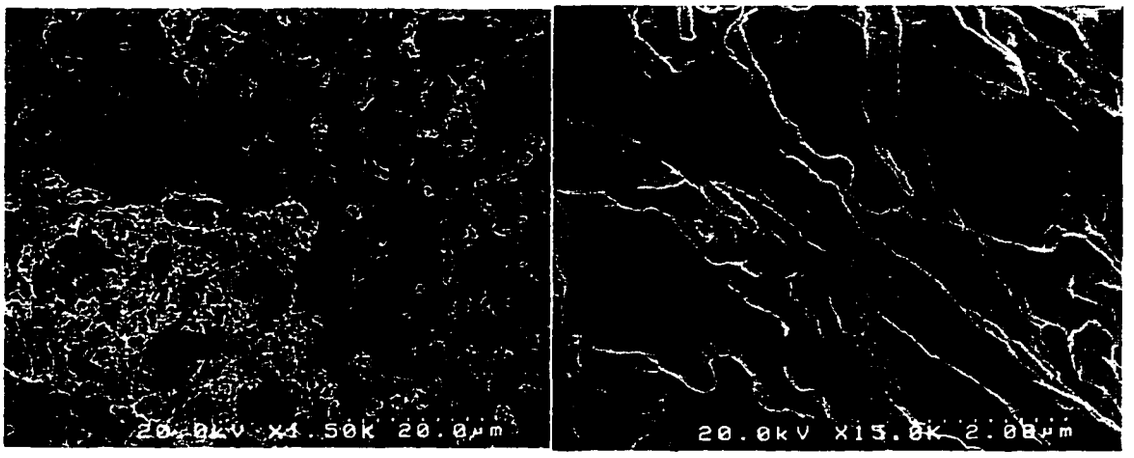

Figure 21. SEM Photographs of Airbrushed Electrode, at 1500X and 15000X

The other two disks were coated by evaporative deposition. The work was done by JPL's Microdevices Lab. The resulting electrodes were 0.5 microns thick, and had a mirror finish. Figure 22 shows a photograph of the disk, and an electron microscope picture of the coating. The evaporation technique produces closely packed columns of platinum. This coating is not porous. Any disk coated in this manner must be put through a conditioning process, as discussed in Chapter 2.

The method used in this study was the slow cycle method discussed by Gur, et al. The system was assembled, and heated to the operating temperature of 1000 °C. The applied voltage was ramped up until the cell voltage reached

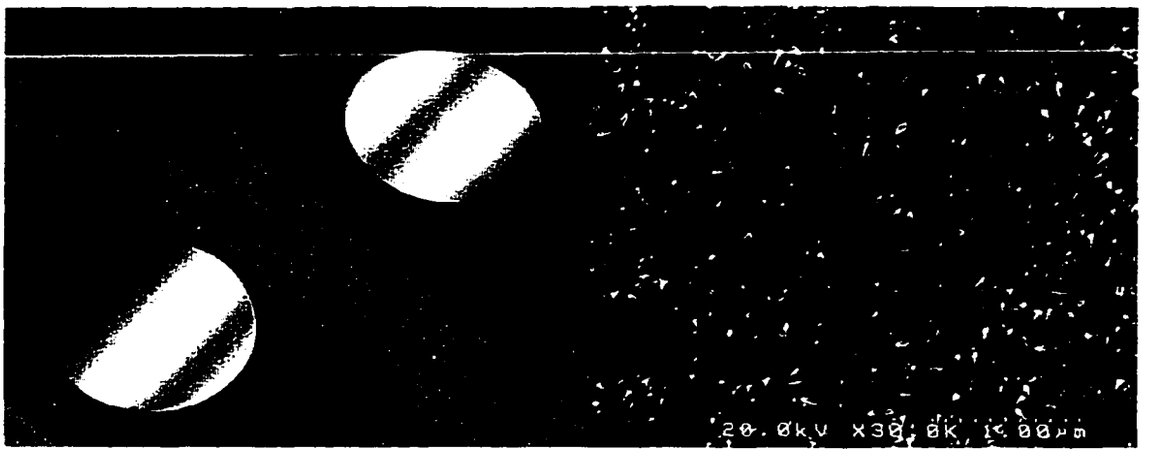

Figure 22. Photo and SEM Photo of Disks with Evaporated Electrodes.

about 1.8 volts. The process was repeated until the hysteresis in the current-voltage plot was either eliminated or reached equilibrium.

After the disks with the JPL electrodes were conditioned, they could be compared with the airbrushed electrodes. The experimental plan was to produce current Vs voltage plots for each electrode, using oxygen, carbon dioxide, and argon as input gases. The argon would provide a baseline for measuring air leaks in the system, and for subtracting their effects. Any current through the circuit when the input gas was argon could only be from air leaking into the system. This series of tests allowed us to compare the performance of the different electrodes. In addition, one disk of each type was run for 120 hours, so any performance degradation over time could be observed.

In all cases, the system is completely characterized by the current flow. Zirconia has an ionic transference number at 1000 °C of 1. Therefore any current through the system can only have been produced by ionic conduction.

It was also desired to have some way to predict cell performance. As seen in Chapter 2, there are as many approaches to this task as there are people making the attempt. It is very difficult to measure some of the parameters necessary to predict the electrochemical process. It was decided to bypass the electrochemistry and take a purely electrical approach, lumping all the electrochemical factors into a constant to be determined by the data.

The starting point for this approach was the electrode. There is a maximum amount of current a conductor can carry, given a voltage difference. The resistance across an electrode will cause the voltage to drop. The analysis was started by assuming that the voltage loss due to current flowing through the z-axis of the electrode is negligible. Current can flow in either the r direction, or be removed into the electrode. Figure 23 shows the model used in this analysis.

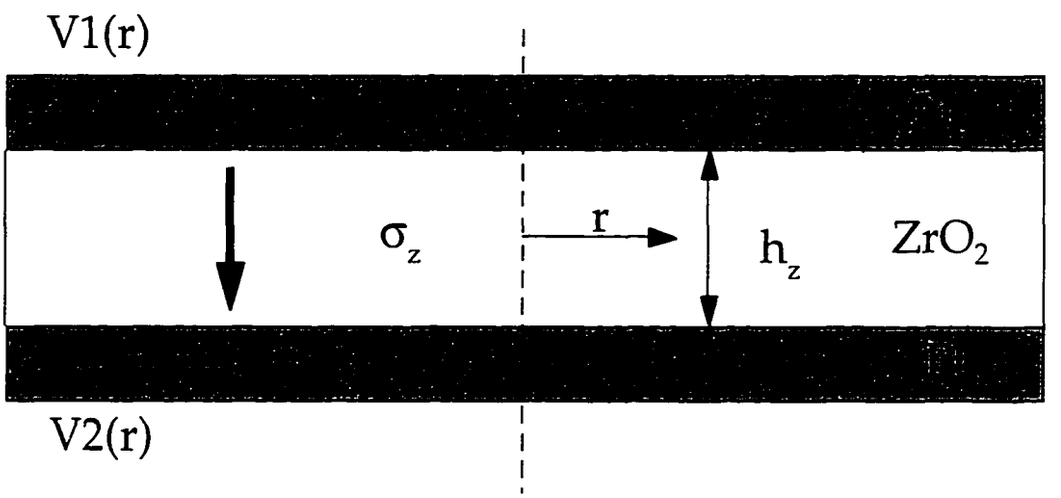

Figure 23. Theoretical Model of Electrode/Electrolyte.

A charge balance for each electrode results in:

$$\frac{d}{dr}\left(2\Pi r h_p j_{p1}\right) = -2\Pi r j_z \tag{12}$$

for the top surface, and

$$\frac{d}{dr}\left(2\Pi r h_p j_{p2}\right) = 2\Pi r j_z \tag{13}$$

for the bottom surface, where r is the radius, h_p is the electrode thickness, j_{p1} and j_{p2} are the current densities in the upper and lower electrodes, and j_z is the current density in the electrolyte. By definition,

$$j_{p1} = -\sigma_p \frac{dV_1}{dr} \tag{14}$$

$$j_{p2} = -\sigma_p \frac{dV_2}{dr} \tag{15}$$

$$j_z = -\sigma_z \frac{dV}{dr} = -\sigma_z\left(\frac{V_1 - V_2}{h_z}\right) \tag{16}$$

where V is the voltage difference across the electrolyte, σ_p is the conductivity of platinum, σ_z is the conductivity of zirconia, and h_z is the thickness of the electrolyte. Substituting these relationships into the charge balance, and assuming that $V_1 + V_2$ is equal to a constant V_0 gives

$$h_p\sigma_p \frac{dV_1}{dr} + r h_p \sigma_p \frac{d^2V_1}{dr^2} = \frac{\sigma_z}{h_z} r\left(2V_1 - V_0\right) \tag{17}$$

If we define

$$A = \frac{\sigma_z}{\sigma_p h_p h_z} \tag{18}$$

the equation simplifies to

$$\frac{d^2V_1}{dr^2} + \frac{1}{r}\frac{dV_1}{dr} = A\left(2V_1 - V_0\right) \tag{19}$$

This equation is known to have a Bessel function solution. The final expression

for the voltage distribution along the top electrode is

$$V_1 = \frac{1}{2}\left[V_0 + \frac{V_0}{I_0\left(\sqrt{2AR}\right)} I_0\left(\sqrt{2A}r\right)\right] \tag{20}$$

where R is the radius of the disk, and I_0 is the modified Bessel function. Similarly, the expression for the bottom electrode is

$$V_2 = \frac{1}{2}\left[V_0 - \frac{V_0}{I_0\left(\sqrt{2AR}\right)} I_0\left(\sqrt{2A}r\right)\right]. \tag{21}$$

The current through the disk can now be found simply by integrating. Results for an applied voltage of V_0=1.4 volts, for an electrode 0.5 microns thick are given in Figure 24. These thicknesses correspond to the evaporated electrodes (JPL#1, and JPL#2).

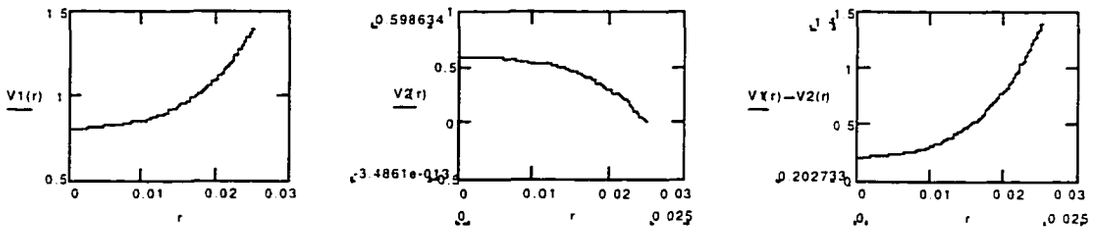

(a) **(b)** **(c)**

Figure 24. Theoretical Voltage Distribution on Electrode Surfaces. (a) Top Surface, (b) Bottom Surface, (c) Voltage Difference Between Surfaces.

Once the voltage distribution is found, the current through the electrode can be found by integrating over the surface of the disk.

$$I = \int_0^R 2\Pi \frac{r}{h_z} \sigma_z (V_1 - V_2) dr \qquad (22)$$

The current found from this equation is greater than the expected values by a factor of about six for carbon dioxide electrolysis, as shown in Figure 25.

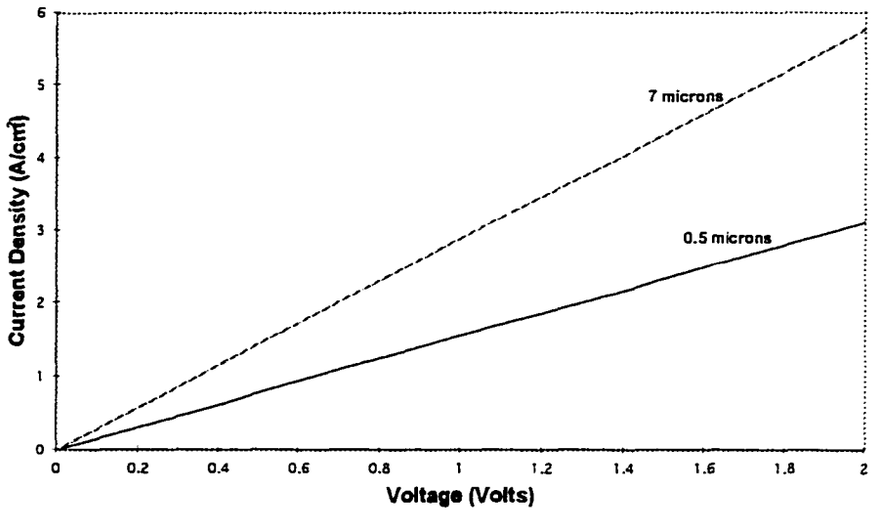

Figure 25. Theoretical Maximum Current Densities.

Electrodes 7 microns thick correspond to the airbrushed electrode, assuming about 30% porosity. The analysis shown above does not account for any of the energy lost in the chemical reaction, or in the diffusion of atoms across the electrode surface. The current equation can be corrected from the experimental data, giving

$$I = \frac{1}{C} \int_0^R 2\Pi \frac{r}{h_z} \sigma_z (V_1 - V_2) dr \qquad (23)$$

where C is a constant curve fit from the data.

The long term tests should show any degradation over time the disks will undergo. It is expected the disks with the thinner electrode will have greater losses with time. As discussed in chapter two, high current levels can change the electrode and electrolyte structures. The thinner electrode will have much higher current densities in the electrode than the thicker coating. The initial level of current should match the values observed in the short term tests.

EXPERIMENTAL RESULTS

Electrode Conditioning

The two disks with the thin evaporated electrodes, JPL#1 and JPL#2, started with 0.5 micron non-porous electrodes. They were conditioned with current to create pores. The voltage-current density plots are shown in Figures 26 and 27.

The first disk, JPL#1, reacted exactly as expected. The first voltage cycle, from 0 to 1.8 volts and down again showed a slight hysteresis. The hysteresis all but disappeared on the second cycle, and there was no indication of it on subsequent cycles. The maximum current density observed was 600 mA/cm^2. The observed resistance of the cell, obtained from the slope of the V-I curve, was 0.2393 Ω.

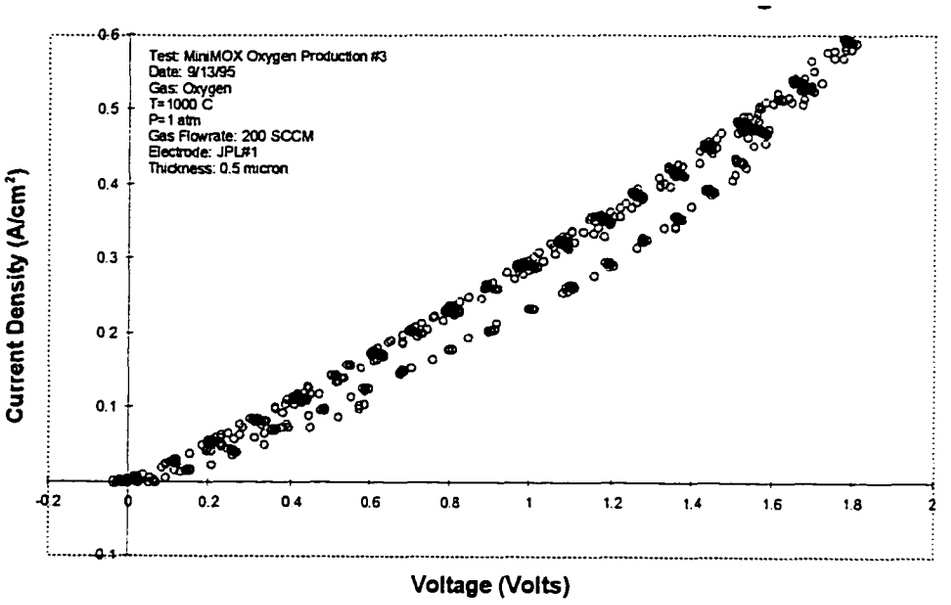

Figure 26. JPL#1 Electrode Conditioning

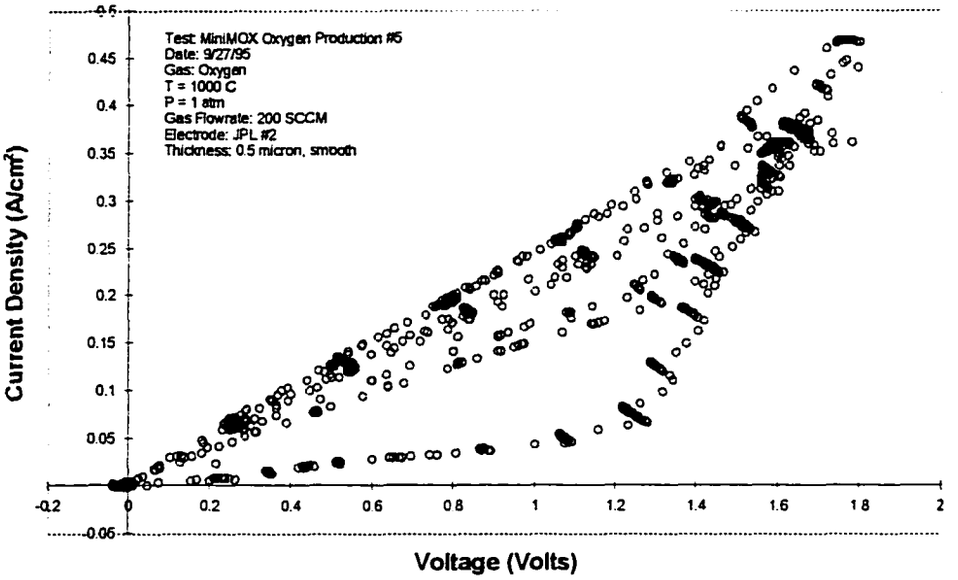

Figure 27. JPL#2 Electrode Conditioning.

The second disk, JPL#2, was the disk used to obtain the SEM picture shown in Figure 22. The electrode was damaged by the tape used to mount the disk in the SEM apparatus. As a result, this disk was expected to show a lower level of performance. The voltage-current density plot shows that more was happening during this test. The initial hysteresis was much greater than seen in the first disk. Also, the hysteresis never went away entirely. It gradually got smaller with each cycle, but remained present. This effect is probably caused by the damage to the electrode. The cell resistance achieved by the end of the test was 0.3063 Ω. The maximum current density was about 475 mA/cm^2. The actual current density was higher, since the total area of the disk was used to calculate this value, when the damaged portion of the disk could not contribute to the process.

Figure 28 shows a voltage-current density plot for the first airbrushed disk, AB#1, as a comparison. This test was run under the same conditions as the tests mentioned above: 200 SCCM of oxygen at 1000 °C. The resistance of the cell with the thicker electrode was 0.2159 Ω, a 10.8% improvement over JPL#1, and a 41.9% improvement over JPL#2.

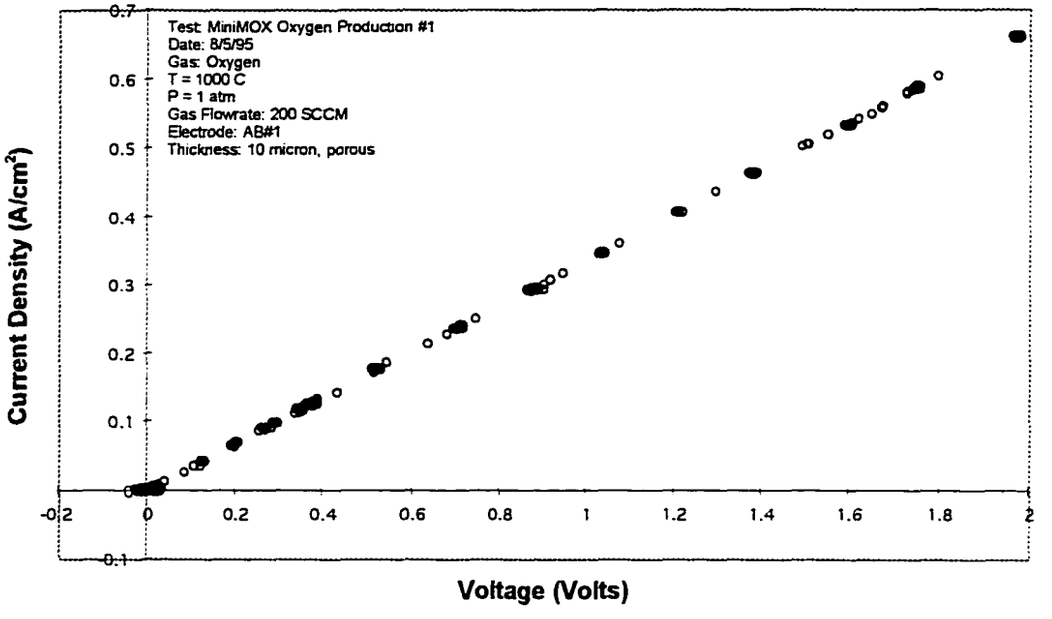

Figure 28. AB#2, Oxygen Transport.

The creation of porosity in disks JPL#1 and JPL#2 obviously is the result of changes in the physical structure of the electrode. The SEM photographs in Figure 29 show the extent of these changes. The cathode side of the disk shows several levels of structure. There are lines of pores 2 microns in diameter dividing the structure into areas 20-30 microns across. On a smaller level, the platinum has formed grains about a micron in diameter, with a network of pores and smaller grains with diameters of about 0.2 microns.

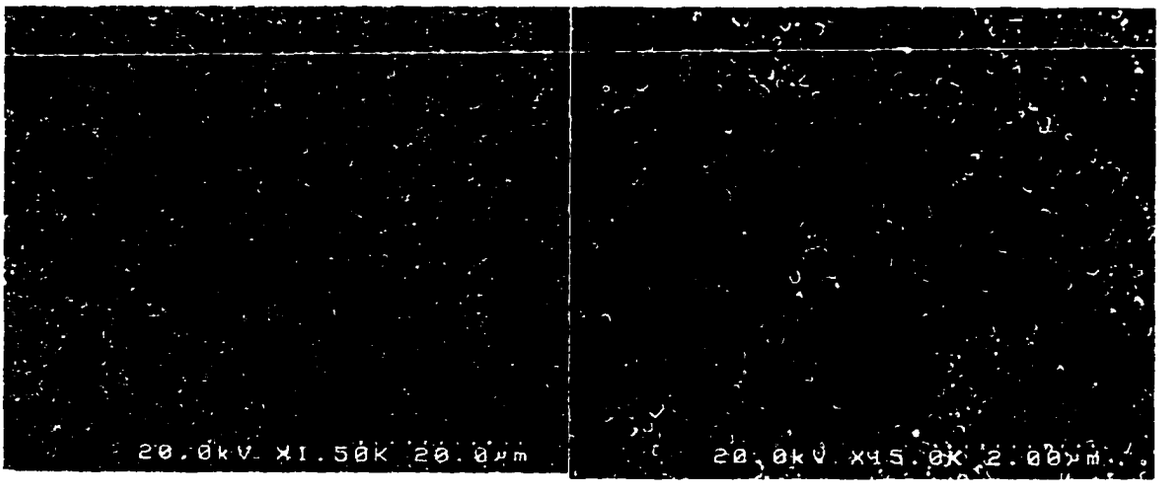

Figure 29. SEM Photos of the Cathode Side of JPL#1, Magnification of 1500X and 15000X

Figure 30 shows the anode side of the disk has a completely different structure. There is detail on only one scale. Both pores and platinum grains are about 1 micron in diameter. The pores are also evenly distributed.

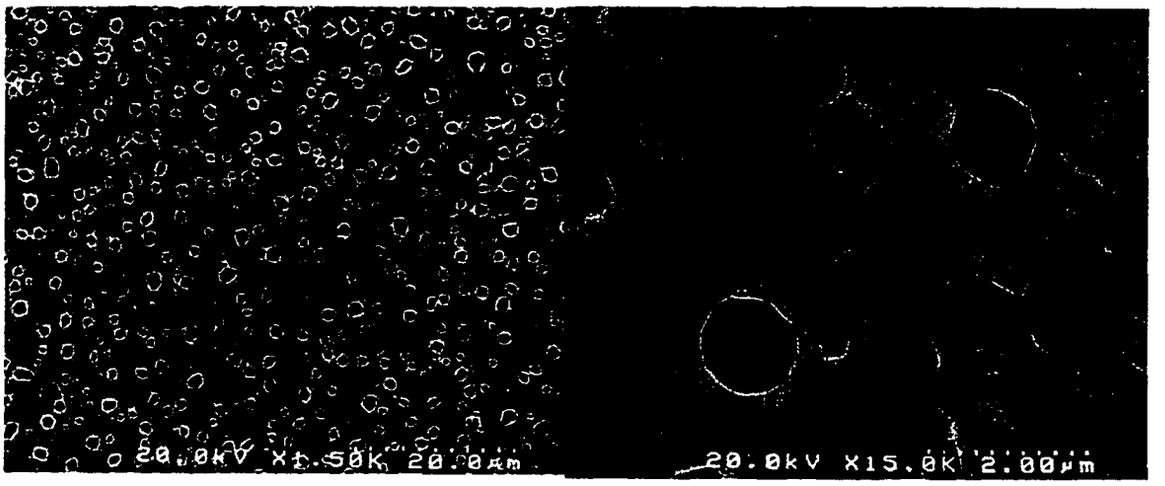

Figure 30. SEM Photos of the Anode Side of JPL#1, Magnification of 1500X and 15000X

The structure differences are caused by the different reactions happening on each side. The cathode side is the location of the electrochemical dissociation of the oxygen atom. The atom then has to find its way to the electrolyte. All that occurs on the anode side is the escape of the oxygen ions. On this side the pores could be caused by the high oxygen pressure between the electrolyte and the platinum forcing splits along grain boundaries. The different reactions cause very different effects in the electrode structure.

The currents calculated in the last chapter are much higher than those seen here. They indicate disk AB#1 should have a current density twice that of the JPL disks. This discrepancy is most likely due to a rate limiting effect. The step that has limited the process has not yet been identified, but some theorectical work to explain the process has been done.[41] The electrochemistry also plays a major role in the reduction of the maximum possible current to the current observed, but this difference will preserve the ratio of currents of the two disks.

Carbon Dioxide Electrolysis

A series of short term tests were performed on some of the electrodes. Disk JPL#1 was cracked following an attempted experiment that failed due to a short in the cell. It was after this test that the zirconia sleeves were added around the bolts. The crack was caused by the increased stress around a spot on the disk where some material got sandwiched between the disk and the MiniMOX top plate.

JPL#2 was put through two short term tests to examine its carbon dioxide electrolysis characteristics. The first test, Mars Oxygen Production #5b (MOP#5b), looked at O_2 and CO_2 electrolysis. MOP#6 looked at the performance with Ar and CO_2. While Ar itself will obviously not produce oxygen, running argon through the system does allow the characterization of leaks.

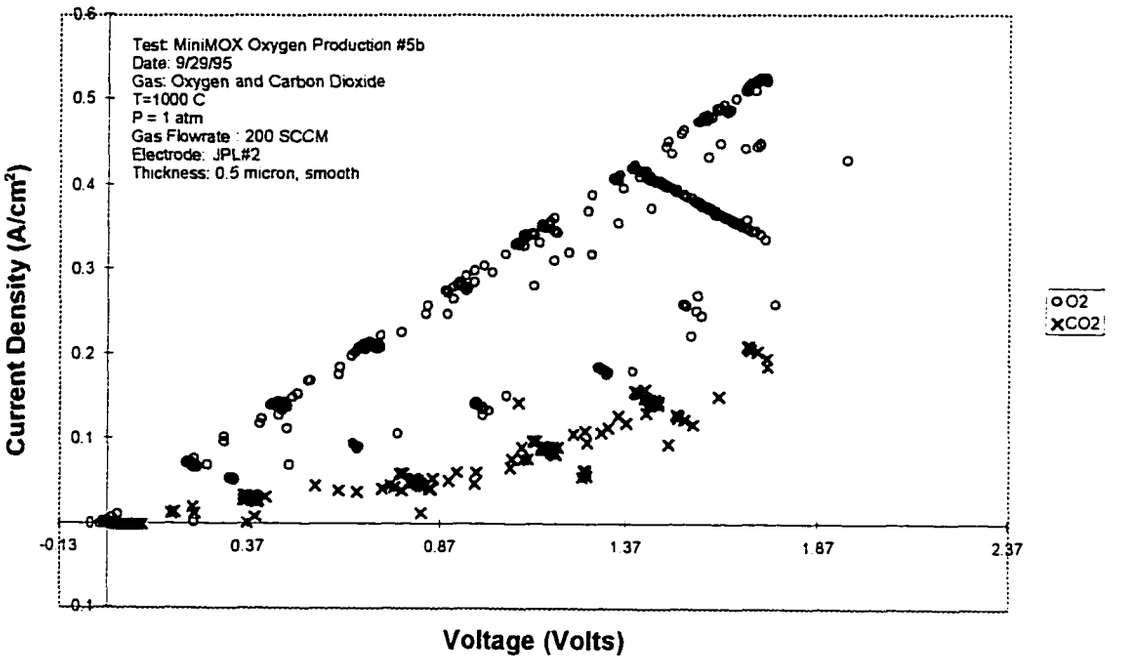

Figure 31. MOP5b Raw Data.

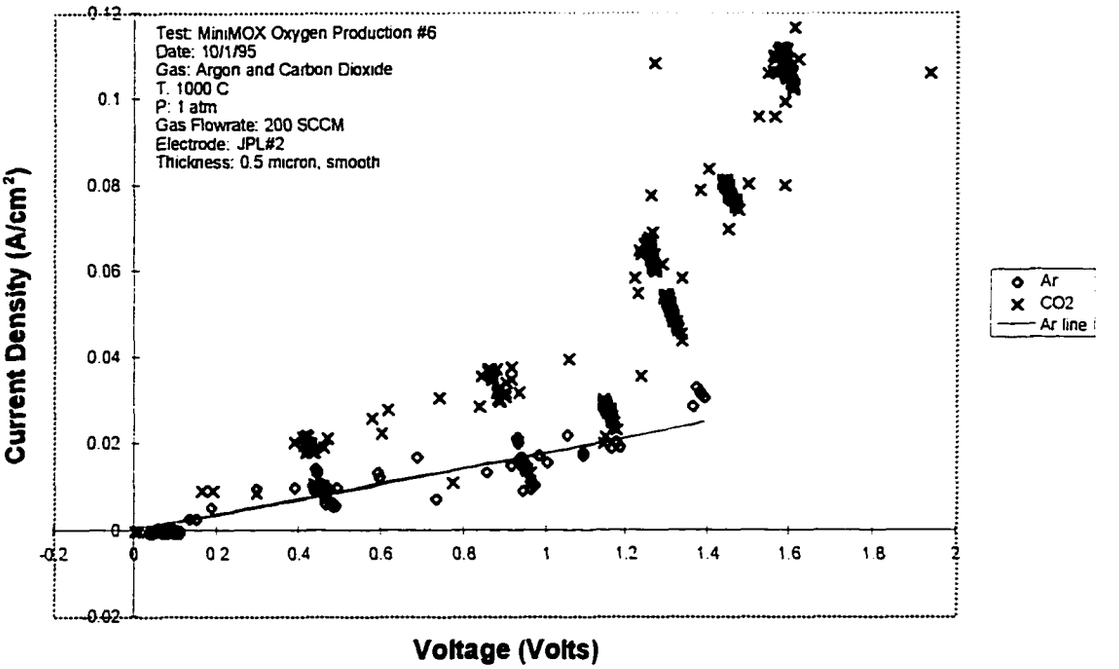

Figure 32. Raw Data from MOP6.

The raw current density data from the two tests is plotted in Figures 31 and 32. From Figure 32 the effect of the argon can be determined. The leak rate for these tests was small, with a maximum of less than 3%, but the oxygen molecules in air are easily transported, so a small leak has a larger effect. The results from MOP#6 show that at 1.4 volts, 0.4 amps of current were transported. This amount is equal to 1.4 SCCM of O_2 from leaks being transported. The slope of the argon line was subtracted from the CO_2 data for both tests. The processed CO_2 data is shown in Figures 33 and 34.

The hysteresis from the damaged electrode is still evident in these tests. The curves also show the bend characteristic of the electrolysis process. The tests were performed by ramping the applied voltage up and down in such a manner to allow the cell voltage to vary between 0 and approximately 1.6 volts.

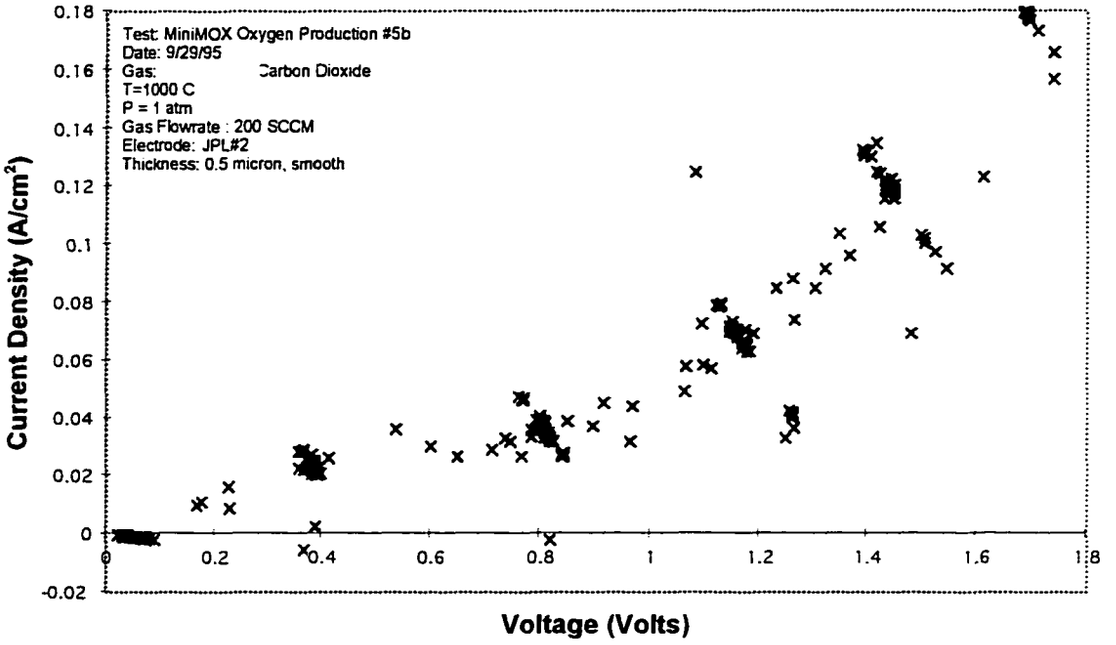

Figure 33. Processed Carbon Dioxide Data, MOP5b.

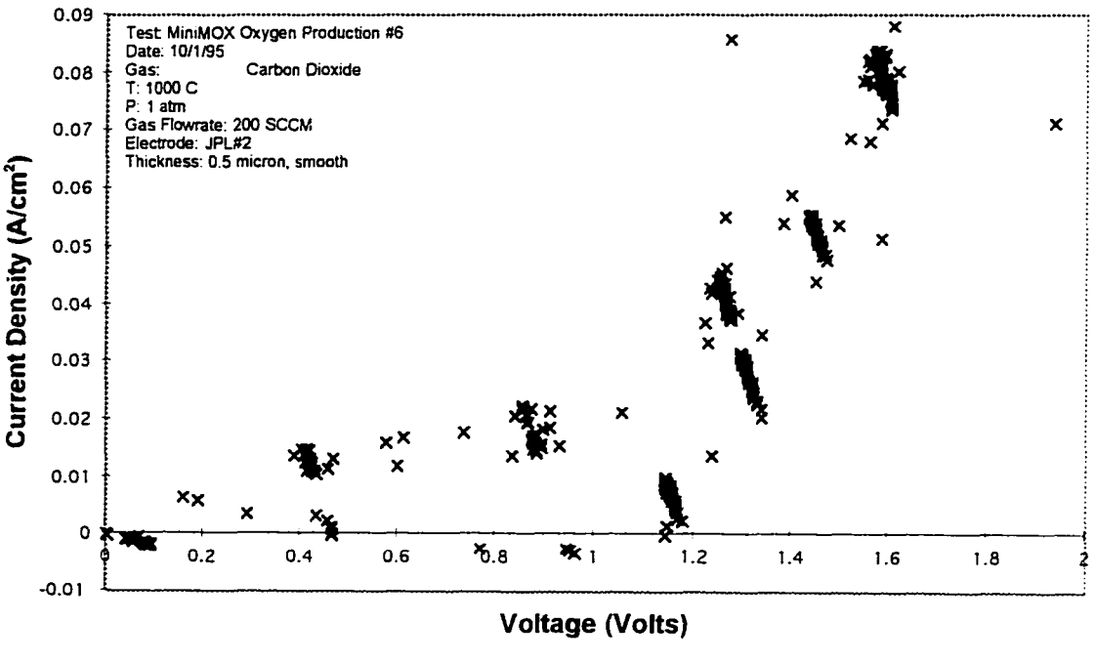

Figure 34. Processed Carbon Dioxide Data, MOP6.

The first ramp up followed the Ar line very closely, indicating that no electrolysis was taking place. In MOP#5b, when the voltage hit 0.75 volts, there is a sharp upturn in the current density, indicating electrolysis has started. The current density never does settle down to the Ar line again. It would be expected that the corrected value of the current would return to near zero for voltages less than 0.75, but it does not. There may be a slow transient effect that did not have time to reach its equilibrium that could account for this data. SOE systems are known to have capacitance like properties.

In MOP#5b, disk JPL#2 was found to have an average resistance of 1.26 Ω for voltages less than 0.75 volts, and a resistance of 0.52 Ω for voltages greater than 0.75 volts. If the hysteresis is taken in to account, the resistances become 1.35 Ω on the way up, and 1.15 Ω on the way down in the low voltage region, and 0.5 Ω going up and 0.53 Ω going down in the high voltage region.

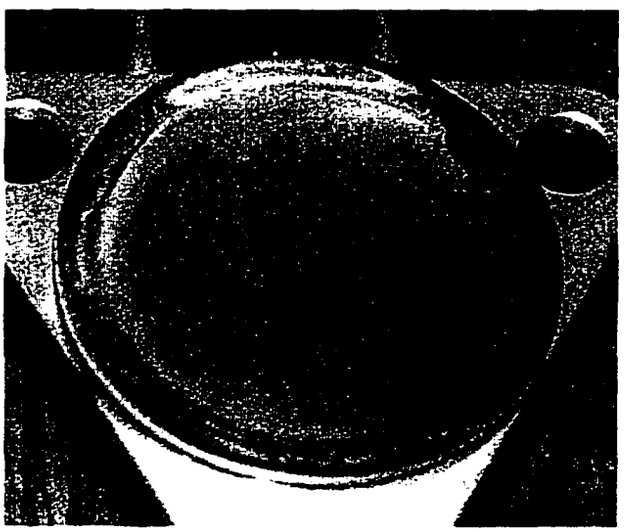

Figure 35. Disk JPL#2, following MOP#6.

The results from the MOP#6 test are much worse. The initial start of electrolysis did not occur until the applied voltage was 1.1 volts. The observed resistances were 3.09 Ω in the low voltage region, and 1.29 Ω in the high voltage region. With hysteresis, the low voltage resistance was 3.3 Ω with increasing voltage and 2.93 Ω with decreasing voltage. For voltages higher than 1.1 volts the increasing and decreasing resistances were 1.34 Ω and 1.29 Ω. These values are more than double the resistances from the previous test. An explanation for these results comes from an examination of the disk. The electrode appears burned over a large portion of the surface. The current may be too high for the thin electrode, an the structure of the electrode has changed from the clouded look it had after conditioning to the look it has now, as shown in Figure 35. The burned areas of the disk would be more resistant than the unburned areas, and the performance of the disk would decline. The damage the disk received during the SEM session is also visible.

The voltage-current relationship of disk AB#2 was examined before and after the disk was put through a 120 hour run. The first test showed substantial improvement over the JPL series electrodes. The data was scattered, but the resistance for the high voltage part of the curve (greater than 0.8 volts), is approximately 0.18 Ω. The scatter on the low voltage side was too great to get a linear correlation. The maximum current density was approximately 240 mA/ cm^2. Figure 36 shows the voltage-current data corrected for air leaks.

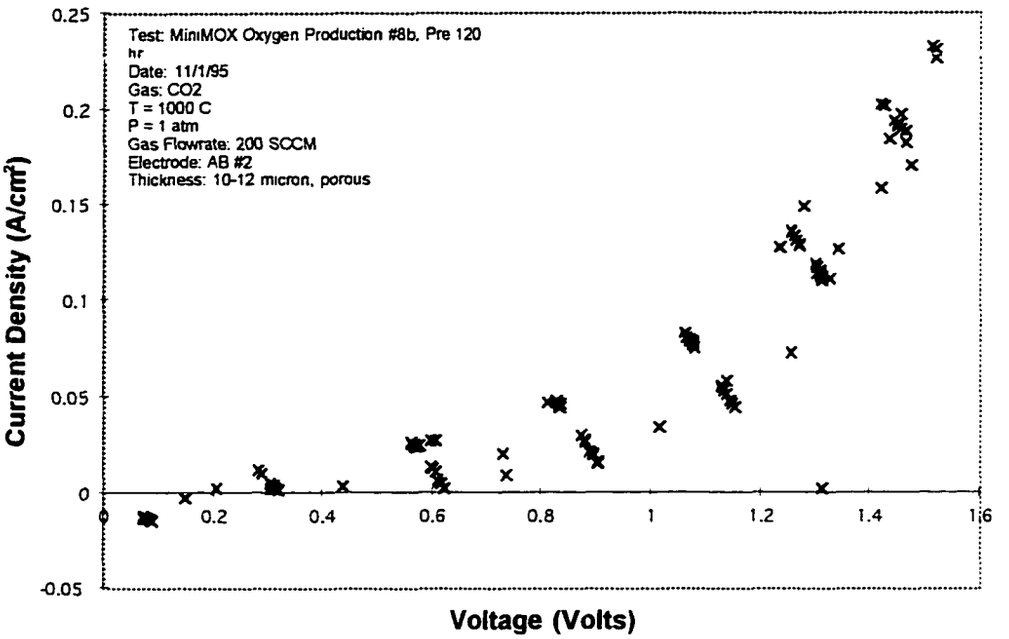

Figure 36. Processed CO_2 Data for Disk AB#2, pre 120 hour test.

The AB#2 test suffered from a large air leak. At high voltages, almost 4 amps of current were being transported just from the air leak. The conclusion that we were dealing with an air leak and not a short, is based on a test in which helium was pumped into the oven. As the helium flow rate was increased, the current dropped. The oven is not sealed so the flow rate needed to compensate for the leak would have exhausted our helium supply in under an hour. It was therefore decided to accept the leak, and characterize its effects.

Figure 37 shows the processed CO_2 electrolysis data for disk AB#2 following the 120 hour test. There is a slight increase in resistance, to 0.19 Ω for the high voltage side. It is likely that the increase in resistance is within experimental error. The maximum current density is about 270 mA/cm^2. The low voltage portion of the curve showed no correlation with the voltage. The air

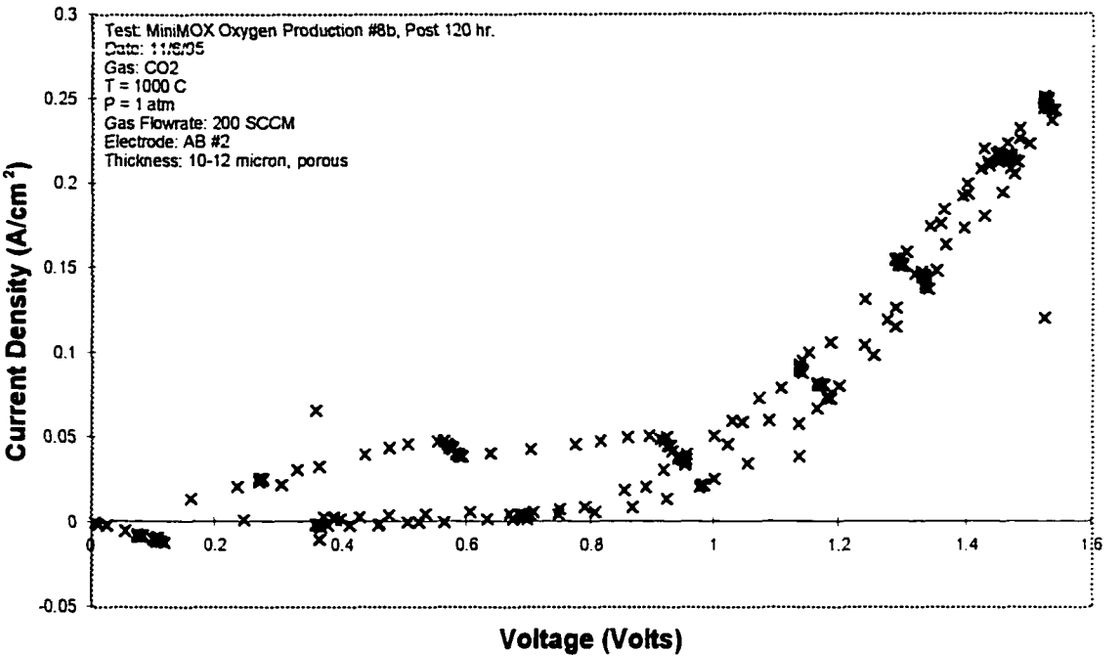

Figure 37. Processed CO_2 Data for Disk AB#2, post 120 hour test.

leak was also reduced during this portion of the test compared to the pre long term test run, being only 57% of the pre test value.

The airbrushed disks showed CO_2 electrolysis resistances of about 1/3 JPL#1, and 1/6 JPL#2. The theory had predicted the resistance was 45% of the JPL disks. However, the thickness of the airbrushed disks varies, so the 7 micron estimate is probably a little low.

The theory from the last chapter does not predict the knee the appears in the CO_2 data. Therefore the value of C can not be predicted from the carbon dioxide data.

Long Term Tests

The first long term test was performed on disk JPL#2. The disk was run with CO_2 as the input gas for 120 hours. The raw voltage and current data vs. time are shown in Figure 38. The air leak was consistently small during this test. Figure 39 shows the processed data. The disk's performance dropped over the 120 hours. By the end of the test the current density had dropped to 40 mA/ cm^2. The CO_2 supply was getting low at this point, so there may have been a reduced flowrate into the cell. The decay rate was steady from the 20 hour mark to the 100 hour mark. During this time, the current decayed at the rate of 1.935×10^{-4} A/hr.

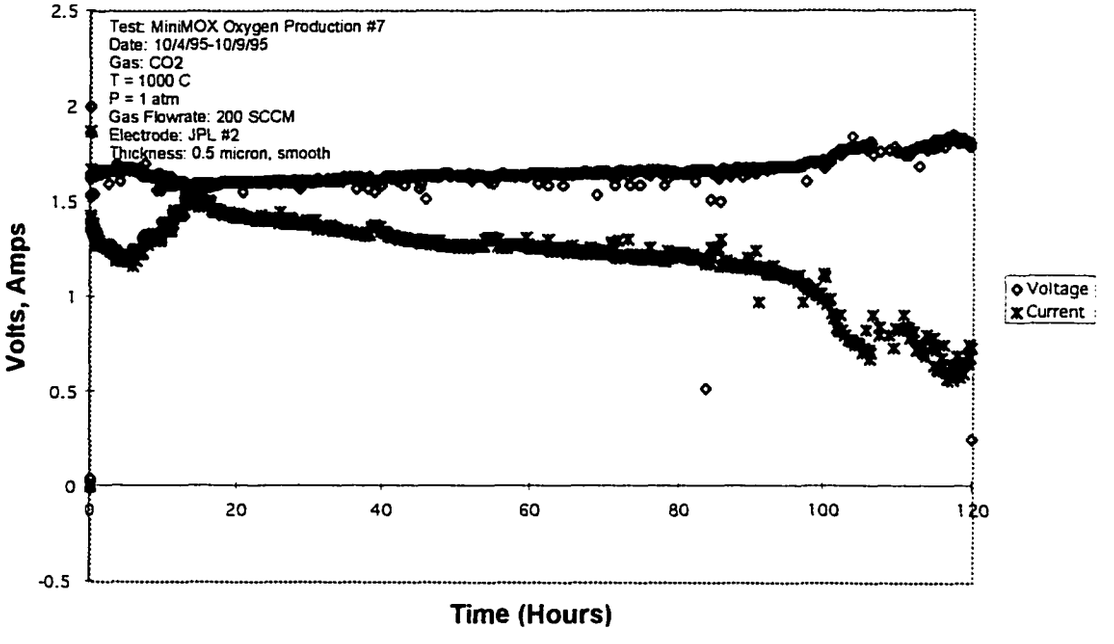

Figure 38. JPL#2, Long Term Test Data.

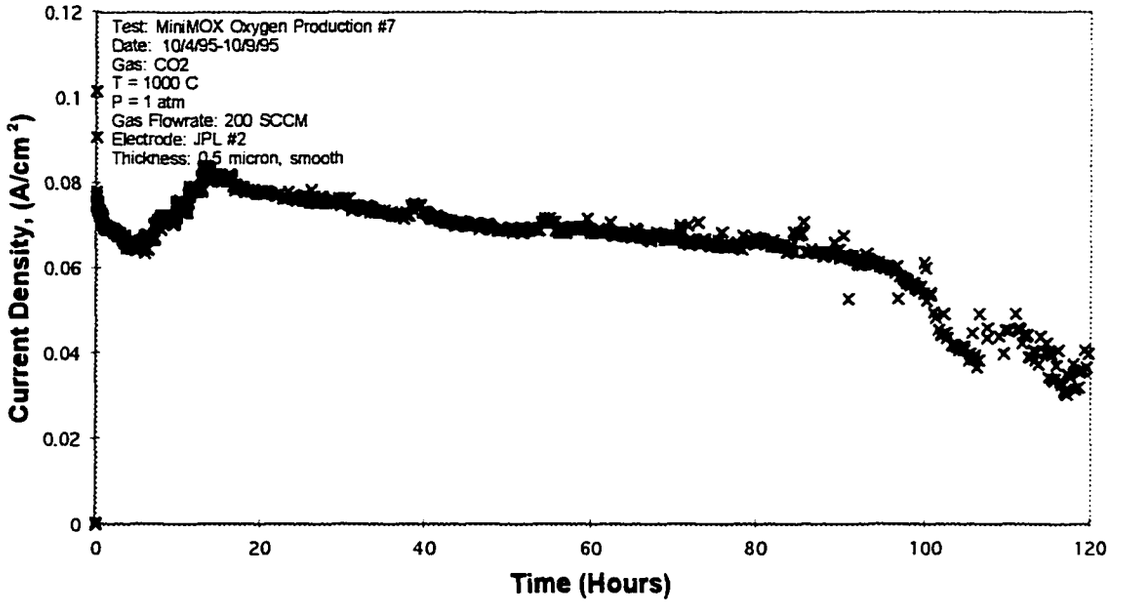

Figure 39. JPL#2, Processed Long Term Data.

Disk AB#2 was also tested for 120 hours. The thicker electrode showed substantially better performance. The raw data in Figure 40 shows a drop in performance, but this is entirely due to the enhanced sealing as the platinum on the disk adhered to the platinum on the MiniMOX plates. The CO_2 electrolysis voltage curves taken before and after the test show that the current density due to CO_2 did not drop. The processed current density data showed no correlation with time, as shown in Figure 41.

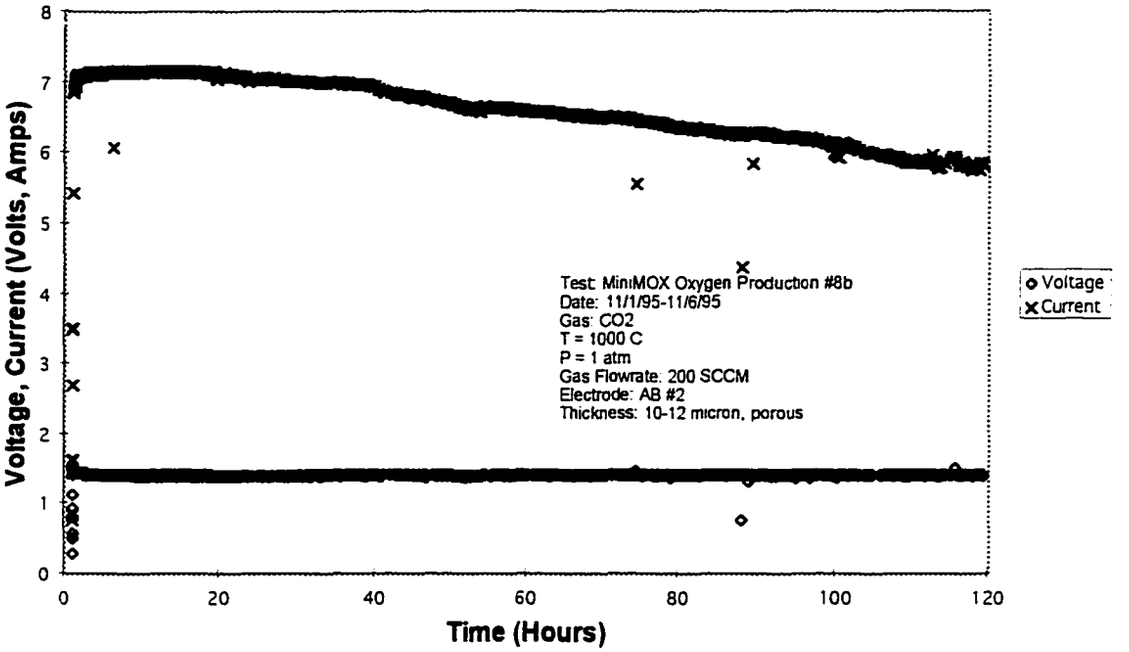

Figure 40. AB#2, Long Term Test Data

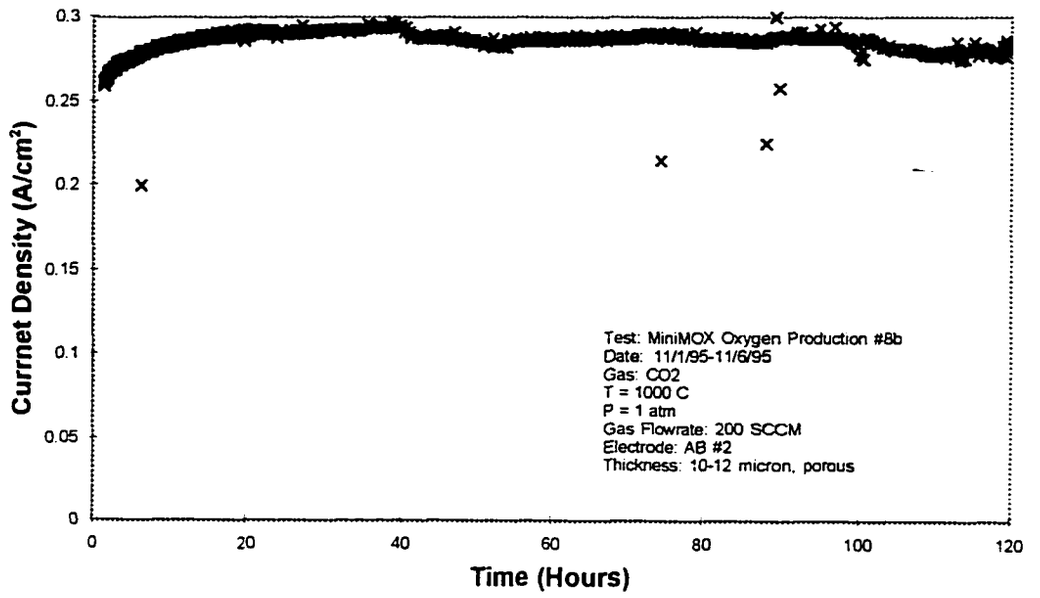

Figure 41. AB#2, Processed Long Term Current Density

MiniMOX System Performance

Throughout these tests, experience has been gained with the MiniMOX system. Several tasks during the assembly of the system before a test must be performed carefully. The bolts must be tightened in such a way that the disk is flush against MiniMOX's plates and air leaks are kept to a minimum. The tubes are very close together, meaning care must be taken to avoid shorting out the cell. Also, the gas line connections must be secure to ensure good electrical contact.

The data acquisition system also must be used with care. The signal conditioner can be temperamental, and frequently will give incorrect readings. These bad data points are easily identified by looking for sudden inconsistent readings in the calculated cell power.

The ammeters used in the system have a combined resistance of 0.23 Ω. In most electronics applications, the currents in use are around 200 mA, with voltages of 5 volts. The resulting loss from the ammeter is negligible in these cases. In this application, the current frequently is above 5 amps, and the voltage is relatively low. The resulting current drop through the ammeter can reach several volts.

As these concerns became known, and the methods of dealing with them were developed, MiniMOX becomes more and more useful. Time between tests has decreased as the system becomes better understood. At the completion of the experiments described in this thesis all of MiniMOX's responses have possible explanations. The next series of experiments to use MiniMOX should go much more smoothly and be completed more quickly.

CONCLUSIONS AND FUTURE WORK

The main conclusion to be drawn from these experiments is that thin electrodes have very poor performance. The thinner electrode can't support the current densities desired, and its performance degrades very rapidly. MOXCE cannot be successful unless the electrode is thick enough to carry the desired current. The long term test clearly show the difference in degradation rates between the thin and thick electrodes. The performance of the JPL disks quickly dropped, finishing with a current density 1/4 of the original level. The airbrushed disks maintained their current density throughout the experiments.

The quality of the electrode also plays an important role. The thicker, airbrushed electrode allowed higher current densities, but also allowed large air leaks. The flat, evaporated electrodes allowed only small leaks. The electrodes used on MOXCE should be deposited in a manner that ensures even thickness around the edge of the disk.

It is also important that ample room exist around the gas and electrical connections in MOXCE. attaching the gas and electrical supply lines proved to be very difficult on MiniMOX. Several problems could have been eliminated by placing the tubes farther apart.

Computer data acquisition played a large part in these experiments. M-DACS allowed long term experiments to be performed without any supervision. No data was lost due to sleep or vacations, or any other human need. Future systems should use an ammeter with a smaller resistance, if possible. The difficulties with data dropout were minor compared with the benefits of having the data taken by the computer.

Despite the minor growing pains MiniMOX suffered, there were significant advances made. MiniMOX shows it is possible to build a high temperature electrochemical apparatus entirely out of metal, except for the electrolyte. By eliminating the need for ceramic parts, the reliability of solid oxide fuel cells and electrolysis systems will be improved. Ceramic materials do not handle multiple temperature cycles well. The use of all metal parts solves this difficulty.

The next step for MiniMOX is the study of disks with hybrid current collector/electrodes. These are created by placing a thick current collector pattern on the disk, and then coating the entire disk with a thin electrode. The thicker areas of the disk will allow increased current, and the thin areas should be small enough to avoid damage from the high current, as well have a reduced voltage drop across them.

This method of electrode preparation should show increased performance over both the thin evaporated electrodes and the airbrushed electrodes. The high current should not damage them, like it does the thin electrodes. The smoother coating will prevent the air leaks of the airbrushed electrodes, and gas will have a thinner layer to pass through. This set of experiments should allow us to design the best electrodes for MOXCE.

After the above set of experiments, MiniMOX can be used concurrently with MOXCE to examine some operating parameters. The ramp up rate for MiniMOX has been set to 3 degrees per minute. This rate is very conservative. Extreme care has been taken to avoid breaking the zirconia crystals through thermal effects. MiniMOX can be used to qualify the disks for faster ramp up rates. Earlier systems, using thicker electrolytes, could be heated to operating

temperature in about 40 minutes, or at a rate of 25 degrees per minute. A ramp up rate this fast will allow tests to be conducted more rapidly than they now are done, with the current 5.5 hour heating period.

Also, the operating pressure for MOXCE has been arbitrarily set at 1 atmosphere. MiniMOX would need to be made airtight to examine pressure effects, but that can probably be accomplished. A better approach might be to replace MiniMOX with a sealed system. Many of the difficulties encountered with MiniMOX were due to the need to take it apart. Once we have a well designed electrode, a single cell testbed can be built that is more like a future flight system would be. By sealing the cell in glass, any leak problem would be avoided. This technique is used in the fuel cell industry for sealing solid oxide fuel cells. A flight system would also be sealed in this manner. With such a system, the effects of pressure and flowrate on the electrolysis process could be studied with much more accuracy than MiniMOX allows.

REFERENCES

1. Clarke, Arthur C., *The Promise of Space*, Pyramid Books, NY, 1968.

2. NASA/JPL, *Our Solar System at a Glance, Information Summary*, PMS 010-a(JPL), JPL 410-34-1, June, 1991.

3. Ash, R.L., Dowler, W.L., and Varsi, G., Feasibility of Rocket Propellant Production on Mars, *Acta Astronautica*, Vol. 5: 1978, p. 705.

4. Richter, R., Basic Investigation into the Production of Oxygen in a Solid Electrolyte Process, AIAA-81-1175, *16th Thermophysics Conference*,1981.

5. Ash, R.L., Richter, R., Dowler, W.L., Hanson, J.A., and Uphoff, C.W., Autonomous Oxygen Production for a Mars Return Vehicle., IAF-82-210, *33rd Congress of the International Astronautical Federation* ,1982.

6. Kaloupis, P., Nolan, P., Cutler, A. Martian Resource Utilization I. Plant Design and Transportation Selection Criteria, *Space Power*, Vol 11: #3 and 4,1992, p.343.

7. Ramohalli, K, Lanton, E., and Ash, R., Recent Concepts in Missions to Mars: Extraterrestrial Processes, *J.Propulsion and Power, AIAA*, Vol. 5: # 2, 1989, p. 181.

8. Space Goals for 21st Century Depicted in Report to White House, *Aviation Week and Space Technology*,Vol. 124: #21, May 26, 1986, p. 16.

9. Ash, R., Huang, J-K., Johnson, P. and Silvertson, Jr., Elements of Oxygen Production Systems Using Martian Atmosphere, AIAA-86-1586, *22nd Joint Propulsion Conference*, 1986.

10. Colvin, J. *A Single-Cell Testbed for Evaluations of Extraterrestrial Oxygen Production*, MS Thesis, University of Arizona, 1993.

11. Gur, T., Wise, H., and Huggins, R., Electrolytic Conversion of Carbon Dioxide to Methane and Oxygen with an Oxygen Ion-Conducting Electrolyte, *Journal of Catalysis*, Vol. 129:1991, p 216.

12. Eliken, L., Archer, D., and Zahradnik, R., Oxygen Regeneration in Solid Electrolyte Batteries: Fundamental Considerations *in Aerospace Life Support, Chemical Engineering Progress Symposium Series, No. 63, Vol. 62*, American Institute of Chemical Engineers, 1966, p. 29.

13. Eliken, L., Morris, J., Wu, C., and Saunders, C., 180-Day Life Test of Solid Electrolyte System for Oxygen Regeneration, ASME 71-36399, *SAE/ASME/AIAA Life Support and Environmental Control Conference*, 1971.

14. Morris, J., Wu, C., Eliken, L., Bifano, N., and Holman, R., Conceptual Design Study of a Six-Man Solid Electrolyte System for Oxygen Reclemation, Westinghouse Electric Corporation.

15. Isenberg, A., Vorostko, C., Carbon Dioxide and Water Vapor High Temperature Electrolysis, SAE Technical Paper Series 891506, *19th Intersociety Conference on Environmental Systems*, 1989.

16. Weissbart, J., Smart, W. and Wydeven, T., Oxygen Reclemation From Carbon Dioxide Using a Solid Oxide Electrolyte, *Aerospace Medicine*, Vol. 40, #2, 1969, p. 136.

17. Isenberg, A., and Cusick, R., Carbon Dioxide Electrolysis with Solid Oxide Electrolyte Cells for Oxygen Recovery in Life Support Systems, SAE Technical Paper Series 881040, *18th Intersociety Conference on Environmental Systems*, 1988.

18. Birnie III, D., *Physical Ceramics, Principles for Ceramic Science and Engineering*, Class Notes, AME 524, Spring 1995.

19. Strickler, D., Carlson, W., Electrical Conductivity in the ZrO_2-Rich Region of Several M_2O_3-ZrO_2 Systems, *Journal of the American Ceramic Society*, Vol. 48, #6, 1965, p. 286.

20. de Dios Solier, J., Perez-Jubindo, M., Dominguez-Rodriguez, A., and Hever, A., Low-Temperature Ionic Conductivity of 9.4-mol % Yttria Stabilized Zirconia Single Crystals, *Communications of the American Ceramic Society*, Vol. 72, #8, 1989, p. 1500.

21. Kilner, J., Brook, R., A Study of Oxygen Ion Conductivity in Doped Non-Stoichiometric Oxides, *Solid State Ionics*, Vol. 6, 1982, p. 237.

22. Etsell, T. and Flengas, s. Overpotential Behavior of Stabilized Zirconia Solid Electrolyte Fuel Cells, *J. Electrochem. Soc.*, Vol. 118, #12, 1971, p. 1890.

23. Casselton, R., Blackening in yttria stabilized zirconia due to cathodic processes at solid platinum electrodes, *Journal of Applied Electrochemistry*, Vol. 4, 1974, p. 25.

24. Bauerle, J. E., Study of Solid Electrolyte Polarization by a Complex Admittance Method. *J. Phys. Chem. Solids*, Vol. 30, 1969, p. 2657.

25. Pizzini, S., General Aspects of Kinetics of Ion-Transfer Across Interfaces *in Fast Ion Transport in Solids* ed. W. vanGool. North Holland/American Elsevier, 1972, p. 461.

26. Gur, T., Raistrick, I., and Huggins, R., Steady-State D-C Polarization Characteristics of the O_2, Pt/Stabilized Zirconia Interface, *J. Electrochem Soc.* Vol. 127, #12, 1980, p. 2620.

27. Klietz, M., Fabry, P., and Schouler, E., Descriptions of Junctions Between Electronic and Solid Ionic Conductors *in Electrode Processes in Solid State Ionics* ed. M Kleitz and J. Dupuy D. Reidel Publishing Company, 1976, p. 1.

28. Raleigh D.O. Electrode Processes in Solid-Electrolyte Systems, *Electroanal. Chem.* Vol. 6, 1972, p. 87.

29. Klietz, M. Electrode and Interface Reactions in Solid State Cells, *Solid State Ionics* Vol. 3/4, 1981, p. 513.

30. Blakely, J. Structure and Defects and Ionic Crystal Surfaces *in Electrode Processes in Solid State Ionics* ed. M Kleitz and J. Dupuy D. Reidel Publishing Company, 1976, p. 83.

31. Sasaki, J., Mizusaki, J., Yamauchi, S., and Fueki, K., Studies on Electrode Processes of Stabilized Zirconia Cells by the Complex Impedance Method, *Solid State Ionics*, Vol.3/4, 1981, p. 531.

32. Pizzini, S., Bianchi, M., Colombo, P. ,and Terchio, S., On the influence of the annealing temperature and heavy current treatments on the porous structure of platinum electrodes and on the kinetics of the oxygen reaction at high temperatures, *Journal of Applied Electrochemistry* Vol. 3, 1973, p. 153.

33. Gur, T., and Huggins, R., Importance of Electrode/Zirconia Interface Morphology in High Temperature Solid Electrolyte Cells *Journal of Applied Electrochemistry* Vol. 17, 1987, p. 800.

34. Isaacs, H., Oliver, C., Schouler, E., and Yang C. Electrode Reactions at Solid Oxide Electrolytes *Solid State Ionics* Vol. 3/4, 1981, p. 503.